Canadian Chemical Transactions Year 2015 | Volume 3 | Issue 2 | Page 118-157

*Review Article*

DOI:10.13179/canchemtrans.2015.03.02.0174

# Emerging Energy Applications of Two-Dimensional Layered Materials

**Dattatray J. Late[1*], Chandra Sekhar Rout[2*], Disha Chakravarty[1] and Satyajit Ratha[2]**

[1]*Physical & Materials Chemistry Division, CSIR-National Chemical Laboratory, Dr. Homi Bhabha Road, Pashan, Pune 411008, India*
[2]*School of Basic Sciences, Indian Institute of Technology, Bhubaneswar, 751013, India*

[*]*Corresponding Author: Email:* dj.late@ncl.res.in, datta099@gmail.com, csrout@gmail.com

***Received:*** *February 19, 2015* ***Revised:*** *March 18, 2015* ***Accepted:*** *March 18, 2015* ***Published:*** *March 22, 2015*

**Abstract:** Atomically thin semiconducting transition metal dichalcogenides (TMDCs) layered materials have recently been emerged as an exciting area of research due to accessibility for easy synthesis using various chemical and physical methods. These two-dimensional (2D) layered materials with single layer have direct and wide band gap due to which, they are more suitable for nanoelectronics and optoelectronics device applications. Here, we present a review of the energy related aspects of atomically thin layered materials like $MoS_2$, $WS_2$, $MoSe_2$, $WSe_2$, InSe, GaSe, GaTe, $MoTe_2$, $WTe_2$ etc. for supercapacitor, solar cell, lithium ion battery and water splitting application. By significantly assessing various materials and comparing their performances with challenging technology, the advantages and disadvantages of this promising area of energy materials are recognized, which may provide guidelines for future progress.

**Keywords:** 2D Nanosheets, Chalcogenides, supercapacitor, Solar cell, Lithium ion battery and Water splitting.

## 1. INTRODUCTION

Bringing forth a sustainable and renewable energy alternative for the future has become a great challenge for scientists, engineers and technologists due to the enormous consumption of global energy and its connection with some critical issues such as climate change. Solar and wind energies are some of the naturally occurring sources which have already provided a well-known platform to generate renewable sources of energy. Among the various energy storage systems, chemical storage devices such as batteries and electrochemical capacitors play major roles for the storage of electrical energy both efficiently and in an environment friendly way. In the last few decades, efforts have been made for an alternative energy storage conversion with high power efficiency and energy densities because of the ever increasing environmental problems due to increased demand for energy and the up-coming diminution of natural resources.[1–4] The 2D layered transition metal dichalcogenide semiconductor materials such as metal oxides and metal chalcogenides have gained the renewed interest. TMDCs consist of hexagonal layers of metal atoms (M= Mo, W, Ga, V, Sn, Ta) sandwiched between two layers of chalcogen atoms (X

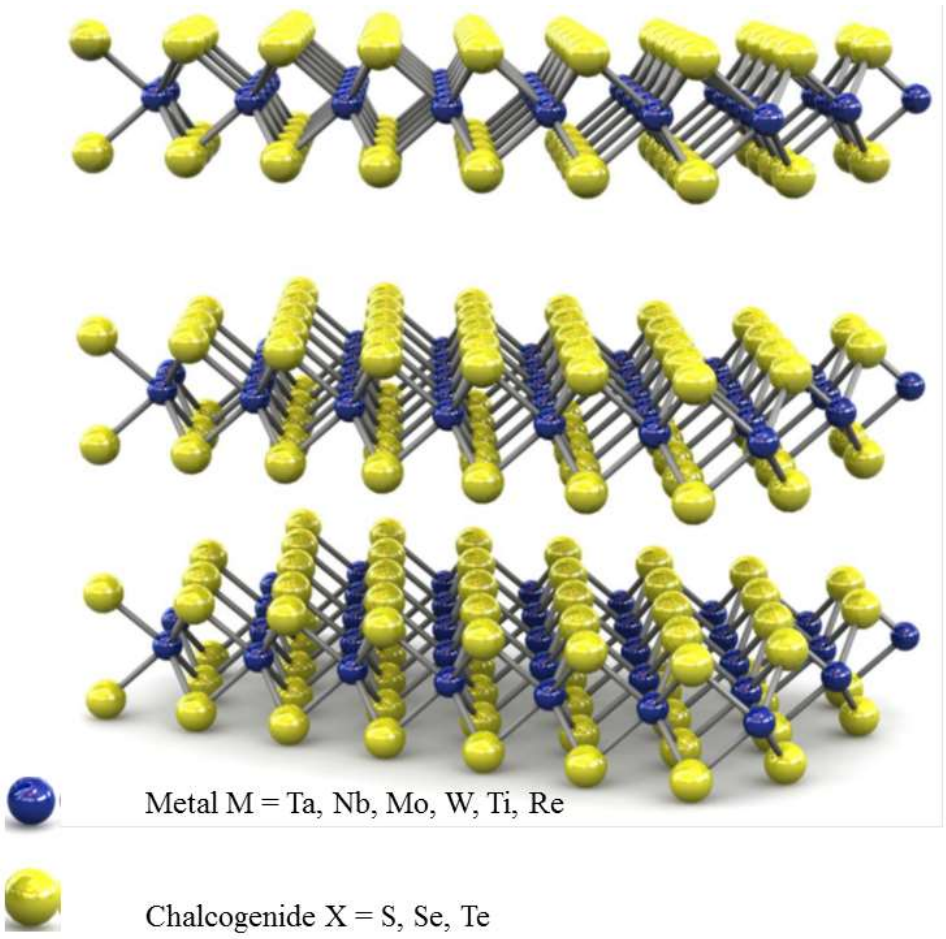


**Figure 1**: 2D Transition metal dichalogenides. (Image taken from ref. 58 Reproduced by permission of the Nature Nanotech).

= S, Se, Te) with an $MX_2$ stoichiometry depending on the combination of chalcogens and transition metals (typically Mo, W, Nb, Re, Ni, or V) as shown in **Figure1**. Among various nanomaterials, transition metal dichalcogenides (TMDCs) have been demonstrated by many researchers to show superior electronic,[5–7] magnetic[8–10] as well as electrochemical[11–13] properties which have attracted great attention for energy related device applications such as supercapacitor,[14–16] solar cell[17–19], lithium ion battery[20,21] and water splitting to generate $H_2$.[22,23] Nanomaterials have excellent properties which enable them to play a crucial role in the rapid progress of the fields of science and technology.[2,24] So far from the literature, it has been realized that 2-D nanomaterials exhibit enhanced electrical, optical and mechanical properties due to their flat geometry. Graphene is already known to show exemplary capability for being highly stretchable (up to 20% elastically),[25–37] having a significantly high carrier mobility ~ $10^5$ $cm^2/Vs$ at 300K,[38–40] transparency ~ 97 %,[41] low density ~ 2 $g/cm^3$,[42] high specific area ~ 2630 $m^2/g$,[43] lightest charge carriers (zero rest mass),[44–46] low cost.[47–50] However the use of graphene has been way too restricted in energy storage device applications due to the absence of a well-defined band-gap. The structures of crystalline TMDCs can be divided into two distinct categories, namely, layered structures with van der Waals gaps[51] representing about two-thirds of TMDCs and otherwise. TMDCs of groups IV

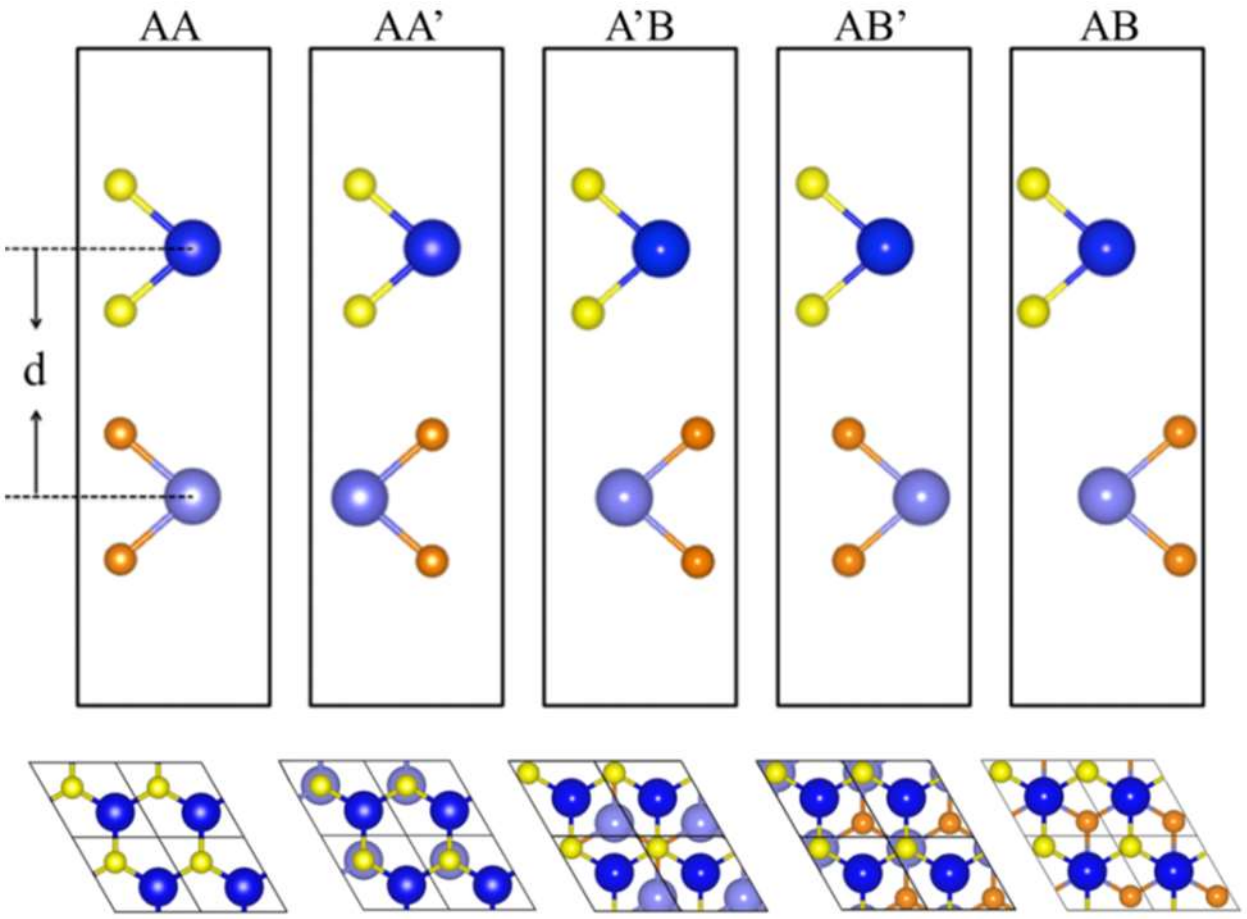


**Figure 2:** Large and small spheres represent the M and X atomic species, respectively. A grayscale (color coding) is used to distinguish the position of the atoms in the two $MX_2$ layers. The full lines demarcate the unit cell (Image taken from ref. 82 Reproduced by permission of the American Physical Society).

($d^2$ electronic configuration), V ($d^3$), VI ($d^4$) and VII ($d^5$) metals tend to form layered structures, while non-layered compounds (e.g., pyrite or marcasite structures) predominantly occur for groups VIIIa–VIIIc ($d^6$–$d^8$) metals. The metal–dichalcogenides ($MX_2$) layered structures arise from the stacking of hexagonally packed planes. The coordination around the metal centers for TMDC layered structures can be either trigonal prismatic (e.g., $MoS_2$, $NbS_2$) or octahedral (e.g., $HfS_2$, $PtS_2$). While bulk $MoS_2$ is an indirect band-gap semiconductor with a band-gap of ~1.2 eV, monolayer $MoS_2$ is a direct band-gap semiconductor with a band-gap of 1.8–1.9 eV.[52–54] Such a transition from an indirect to a direct band-gap semiconductor is also observed in other inorganic layered materials,[55–59] making such $MX_2$ monolayers in nanoelectronics applications superior to pristine graphene that has no band-gap. Intriguingly, the presence of several conduction and valence band valleys in graphene could open up the way towards the realization of valleytronics devices, based on the possibility of selectively confining the charge carriers in a restricted portion of the momentum space[60–62]. As TMDCs have well defined band-gaps which also can be tuned by controlling the number of layers. These layered materials also have a wide absorption range such as visible, infrared, ultraviolet and near infrared, so they possess this unique property of getting self-excited

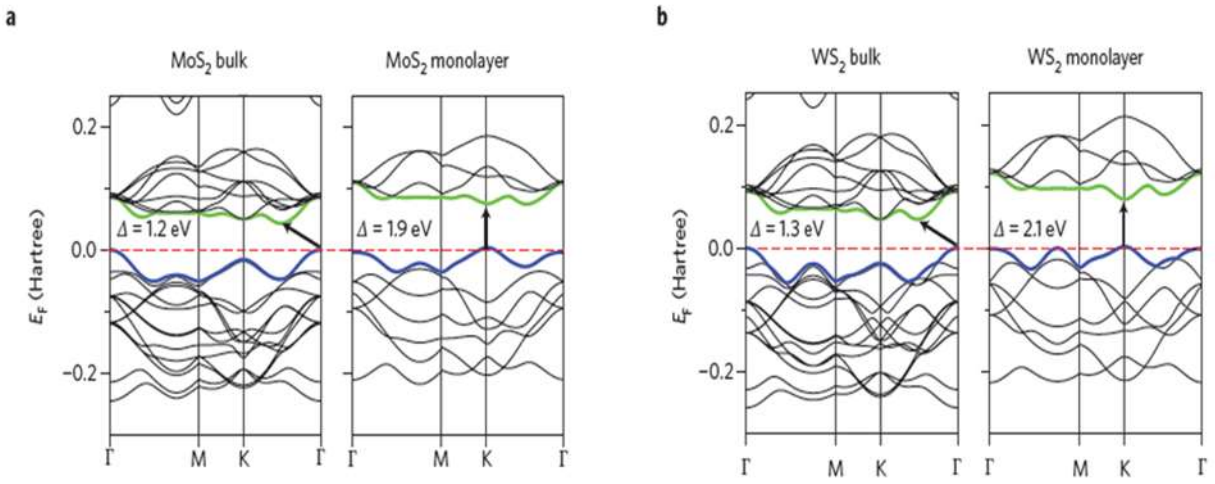


**Figure 3 :** Electronic properties and band structure of TMDCs. Band structures calculated from first-principles density functional theory (DFT) for bulk and monolayer $MoS_2$ (a) and $WS_2$ (b). (Image taken from ref. 58 reproduced with permission from Nature Nanotechnology).

under light irradiation. Recent experimental and theoretical investigations on $MoS_2$ demonstrate that the phonon dispersion relations[63] as well as the band gap and exciton binding energies[64–66] show interesting quantum confinement effects[67], when the layer thickness is reduced. Secondly, the large surface area of 2D graphene-analogue materials could supply more surface active sites and increase the adsorption of the substrates. The 2D planar structure, large surface area, and especially its insignificant thickness could be beneficial for reducing the recombination of the photo-generated electrons and holes. Therefore, the layered TMDC materials show interesting photoelectric and catalytic properties[68,69].

## 2. Properties of Layered Semiconducting TMDCs:

### 2.1 Physical Properties of TMDCs:

The semiconducting dichalcogenide material, $MX_2$, is a promising material for electronic applications because of its high stability and transport characteristics. Unlike graphene, these compounds don't actually consist of a single layer of atoms. Rather, they comprise a layer of transition metal atoms sandwiched between two layers of chalcogen atoms. Hexagonal $MoS_2$[70,71], $WS_2$[72,73], $MoSe_2$[72,74], $WSe_2$[75],GaS[76,77], GaSe[76,77] and etc. have layered structures with each layer having X–M–X or X-M-M-X kind of structural arrangement. Natural or synthetic $MX_2$ crystallizes in two different polytypisms, 2H (space group: $P6_3/mmc$) and 3R (space group: R3m), with the former being the dominating one. In both phases the M atom in one layer is aligned over the X atom in the layer beneath, but the lateral registry is different: in 2H, the X atoms are fully eclipsed, whereas in the 3R geometry, the X atoms are staggered, i.e., one X is eclipsed by the M atom above and the second one is located below the hexagonal hollow site[13,78,79], resulting in the staggered AB stacking as shown in **Figure 2**.

The high-symmetry stacking orders are depicted in **Figure 2**: (i) AA (point group $D_{3h}$), eclipsed stacking with M over M and X over X; (ii) AA (point group $D_{3d}$), eclipsed stacking with M over X, characteristic of the 2H phase; (iii) AB (point group $D_{3d}$), staggered stacking with X over X; (iv) AB (point group $C_{3v}$),

staggered stacking with X over M, characteristic of the 3R phase; (v) AB (point group $D_{3d}$), staggered stacking with M over M. It is readily seen that one can transform one stacking polytypism into another by horizontal layer sliding and/or by rotation around the vertical axis[80]. Taking $MoS_2$ as an example, naturally occurring $MoS_2$ has two polytypes, 2H and 3R, both having the trigonal prismatic coordination.[81,82] The structure of $MoS_2$ consists of an atomic plane of Mo sandwiched between two atomic planes of S in a trigonal prismatic arrangement S–Mo–S. The bond distance of S–Mo is 1.54 Å and S–S is 3.08 Å[77].

**2.2 Electronic band Structure of TMDCs:**

Many TMDCs have band structures that are similar in their general features, as shown by first principles and tight-binding approximations[71,83–88] and measured using a variety of spectroscopic tools[89–92]. In general, $MX_2$ compounds are semiconducting whereas $VX_2$, $NbX_2$ and $TaX_2$ are metallic[53,85,86,89–94]. The electronic band structure properties of semiconducting TMDCs also depend on the number of layers due to quantum confinement effects and changes in symmetry[71,95]. Several groups have predicted and verified the transition from an indirect band gap at the Γ-point to a direct band gap at the K-point of the Brillouin zone as the thickness of semiconducting TMDCs is reduced to a single layer[57,94]. In particular, bulk $MoS_2$ has an indirect band gap of 1.2 eV, whereas single layer $MoS_2$ has a direct band gap of 1.9 eV as shown in **Figure 3.**

This leads to an observation of enhanced photoluminescence (PL) in case of $MoS_2$[96–99]. Similar evidence for a direct band gap transition has also been reported for single layer $MoSe_2$, $WS_2$, and $WSe_2$[100,101]. At the Γ-point, the bandgap transition is indirect for the bulk material, but gradually shifts to be direct for the monolayer[102–106]. The direct excitonic transitions at the K-point remains relatively unchanged with layer number. The change in the band structure with layer number is due to quantum confinement and the resulting change in hybridization between $P_z$ orbitals on S atoms and d orbitals on Mo atoms[71,84,96]. The electronic distributions are also spatially correlated to the atomic structure. For $MoS_2$, DFT calculations show that the conduction-band states at the K-point are mainly due to localized d orbitals on the Mo atoms, located in the middle of the S–Mo–S layered structure and relatively unaffected by interlayer coupling. However, the states near the Γ-point are due to combinations of the antibonding $P_z$-orbitals on the S atoms and the d orbitals on Mo atoms, and have a strong interlayer coupling effect[96]. Therefore, as the layer number changes, the direct excitonic states near the K-point are relatively unchanged, but the transition at the Γ-point shifts significantly from an indirect to direct. All $MX_2$ compounds are expected to undergo a similar indirect band-gap to direct band-gap transformation with decreasing layer numbers, covering the bandgap energy range 1.1–1.9 eV[64,85–88,107,108]. The electronic band structures of semiconductors directly influence their ability to absorb and emit light. For semiconductors with a direct bandgap, photons with energy greater than the bandgap energy can be readily absorbed or emitted. For indirect bandgaps, an additional phonon must be absorbed or emitted for the sake of conservation of crystal momentum, making the photon absorption or emission process much less efficient[109,110].

**2.3 Mechanical properties of TMDCs:**

The TMDCs attract great interest and importance to examine the mechanical properties of the other 2D nanomaterials. Mechanical properties of TMDCs materials are usually defined by the unit-cell geometry, the relative density ($\rho = \rho/\rho_s$) and the solid material properties[111]. Castellanos-Gomez *et. al.*[112] measured the elastic properties of freely suspended $MX_2$ nanosheets, with thicknesses ranging from 5 to 25 layers. The measurement was performed by using an AFM tip, which applied load at the center of the

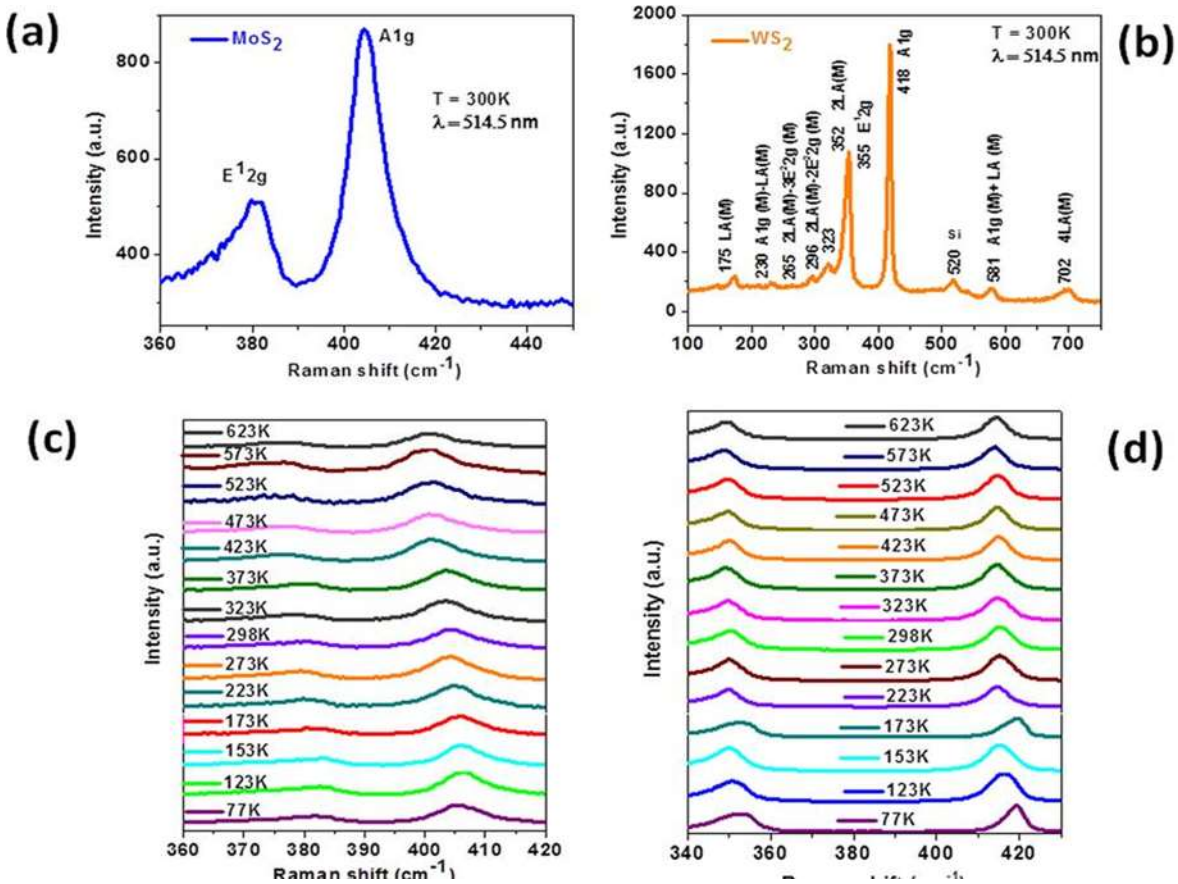


**Figure 4**: Room temperature Raman spectra of a few layers (a) $MoS_2$ and (b) $WS_2$. Temperature dependent Raman spectra of few-layer samples of (c) $MoS_2$ and (d) $WS_2$. (Image taken from ref.119, Reproduced by the permission of AIP from Appl. Phy. Lett. 2014).

suspended region of a $MoS_2$ nanosheet. The displacement of the AFM scanning piezo and ΔZc is the deflection of an AFM cantilever. It is reported that the average Young's modulus of the $MoS_2$ sheet is exceptionally high, i.e. E = ~0.33±0.07 TPa, which is comparable to that of graphene oxide. This value is also higher than the Young's modulus of bulk $MoS_2$ (i.e. ~0.24 TPa), most likely resulting from the lower density of stacking faults present in thinner flakes compared to the bulk crystal[113]. Moreover, these nanosheets exhibited low pre-strain and could stand elastic deformations up to tens of nanometers without breaking. Another work carried out by Bertolazzi *et. Al* shows a Young's modulus of ~0.27 TPa for a monolayer $MoS_2$, lower than that of multi-layers, but higher than that of the bulk form. It was also found that the measured strength of individual single-layer $MoS_2$ was in the range of 6–11% of its Young's modulus, which is at the theoretical upper limit of a material's breaking strength (i.e. The intrinsic strength of interatomic bonds in the crystal)[114,115]. The excellent elastic properties of single-layer and multi-layer dichalcogenides nanosheets make them attractive semiconductors for flexible electronic and optoelectronic devices, as well as for composite films.

### 2.4 Optical and vibrational properties of TMDCs:

When the thickness of TMDCs is reduced from bulk to monolayer, an indirect to direct band gap crossover, which is a ubiquitous effect in layered semiconductors. During this crossover, the band gap

becomes degenerate for bilayer $WSe_2$, which is also similar to the soft crossover observed in $MoSe_2$. The Raman spectra of bulk $WSe_2$ possesses a prominent peak at 250 $cm^{-1}$ and flakes thinner than quadro-layers exhibit an additional peak at ~10 $cm^{-1}$ more than that of the first order peak[116,117]. Phonon dispersion calculations indicate that the $E_{2g}$ and $A_{1g}$ modes are degenerate and hence yield a strong Raman peak at 250 $cm^{-1}$ but these modes remain degenerate independent of the thickness for few layered $MoS_2$ and $WS_2$. The Raman peak positions of both $A_{1g}$ and $E^1_{2g}$ modes shift to lower wave-number when temperature increases from 77K to 623 K. Raman spectrum of a few layer $WS_2$ nanosheets excited with 514.5 nm laser source was rich in information which reveals many first-order and second order modes: LA (M) appears at 175 $cm^{-1}$, 2LA (M) mode appears at 352 $cm^{-1}$, $E^1_{2g}$ appears at 355 $cm^{-1}$, and $A_{1g}$ appears at 418 $cm^{-1}$. It is observed that the intensity of $A_{1g}$ mode is twice than that of the $E^1_{2g}$ mode. It is also important to note that 2LA (M) mode and $E^1_{2g}$ mode overlap with each other. **Figures 4(a) and 4(b)** show the Raman peak position shift in $E^1_{2g}$ and $A_{1g}$ mode as a function of temperature for a few layer of thick $MoS_2$ nanosheet sample[118].

It is reported that 1% uniaxial strain which is likely to be present as a result of substrate-sample interaction[119]. For biaxial strain, the degeneracy is still preserved but once uniaxial strain is applied, i.e. crystal symmetry is broken, the degeneracy is lifted and the calculated phonon dispersion matches closely to experimental observations[57,120–122]. The phonon structure of semiconducting TMDCs is also sensitive to the number of layers and strain as well as temperature and carrier concentration. The Raman spectra of TMDCs contain two predominant and distinct peaks : (1) The out-of-plane $A_{1g}$ mode where the top and bottom X atoms are moving out of plane in opposite directions while M is stationary; (2) The in-plane degenerate $E^1_{2g}$ mode where the M and X atoms are moving in plane in opposite directions. The addition of extra layers leads to stiffening of the out-of-plane phonon modes and relaxation of in-plane bonding, resulting in a blue shift of the $A_{1g}$ mode and a red shift of the $E^1_{2g}$ mode[65,123.] Both of these modes undergo a red shift as well as spectral broadening with increasing temperatures that is attributed to certain amount of harmonic contributions towards the interatomic potentials[124–126]. The $A_{1g}$ mode is also sensitive to carrier density and undergoes a red shift as well as peak broadening with electron doping while the $E^1_{2g}$ mode remains insensitive to doping, suggesting stronger electron-phonon coupling with the out-of-plane vibrational mode[127]. The same effect is also evident in resonant Raman spectra of TMDCs where the intensity of the $A_{1g}$ mode is greatly enhanced under resonance conditions while the enhancement vanishes with reduced thickness due to reduced electron-$A_{1g}$ phonon coupling in thinner samples. Resonance conditions have also led to the observation of a new second-order longitudinal acoustic (LA) phonon mode, the intensity of which increases upon reduction in the sample thickness[93]. While the $E^1_{2g}$ mode remains insensitive to doping, it is very sensitive to applied strain. Applying uniaxial strain lifts the degeneracy of the $E^1_{2g}$ mode, leading to red shifting and splitting into two distinct peaks for strain of just 1%[128]. The unique electronic band structure and lattice vibration properties of TMDCs suggest new opportunities for electronic, optoelectronic, and sensing devices. Thus the application of strain appears to be a promising approach for a rapid and reversible tuning of the electronic, vibrational and optical properties of single layer $MX_2$ dichalcogenides. The band-gap, mobility of single-sheet, semiconductor type and Spectral Range, responsivity of the various TMDCs are tabulated in Table 1 in detail.

**Table 1.** The characteristic of TMDCs semiconductor materials, the bandgap, mobility, semiconductor type, spectral range and responsivity are shown.

| TMDCs | Band-gap (eV) | Mobility of single-sheet $cm^2V^{-1} s^{-1}$ | Semiconductor type | Spectral Range | Responsivity (mA/W) | Ref. |
|---|---|---|---|---|---|---|
| $MoS_2$ | Indirect-1.29<br>Direct-1.8 | 517 | n-type | Visible | 7.5 | [129–132] |
| $WS_2$ | Indirect-1.35<br>Direct-1.1 | 19 | n-type | Visible | 2.0 | [101,133–135] |
| $MoSe_2$ | Indirect-1.1<br>Direct-1.55 | 70 | n-type | UV-vis-NIR | 10 | [135–137] |
| $WSe_2$ | Indirect-1.2<br>Direct-1.8 | 250 | n-type | Visible | 210 | [101,137,138] |
| $MoTe_2$ | Indirect-1.00<br>Direct- 1.10 | 170 | p-type | UV-vis-NIR | 12 | [135,139] |
| $WTe_2$ | Indirect -0.81<br>Direct - 1.18 | - | n-type | - | - | [140,141] |
| GaTe | Indirect-1.13<br>Direct-1.7 | 0.20 | p-type | Visible | $10^{-4}$ | [142] |
| InSe | Direct-1.3 | ~1000 | n-type | Visible | 12300 | [143–147] |
| GaSe | Indirect-0.99<br>Direct-2.352 | 1-5 | p-type | Visible | - | [76] |
| Black Phosporous | Direct-1.8 | 1000 | p-type | Visible | - | [148] |

The electron mobility is characterized on the basis of how fast an electron can travel through metal/semiconductor after applying an electric filed. In a semiconductor, the carrier mobility were referred for the mobility of both electron as well as hole. For a photoconductive mode, the spectral responsivity is defined as the ratio of the generated photocurrent to incident light power, which is expressed in A/W.

**3. Synthesis of layered Transition metal dichalcogenides:**

Literature survey reveals that till date, both physical and chemical approaches have been utilized effectively for the synthesis of TMDCs[149,150]. This section gives brief overview of various recent synthesis methods of 2D materials.

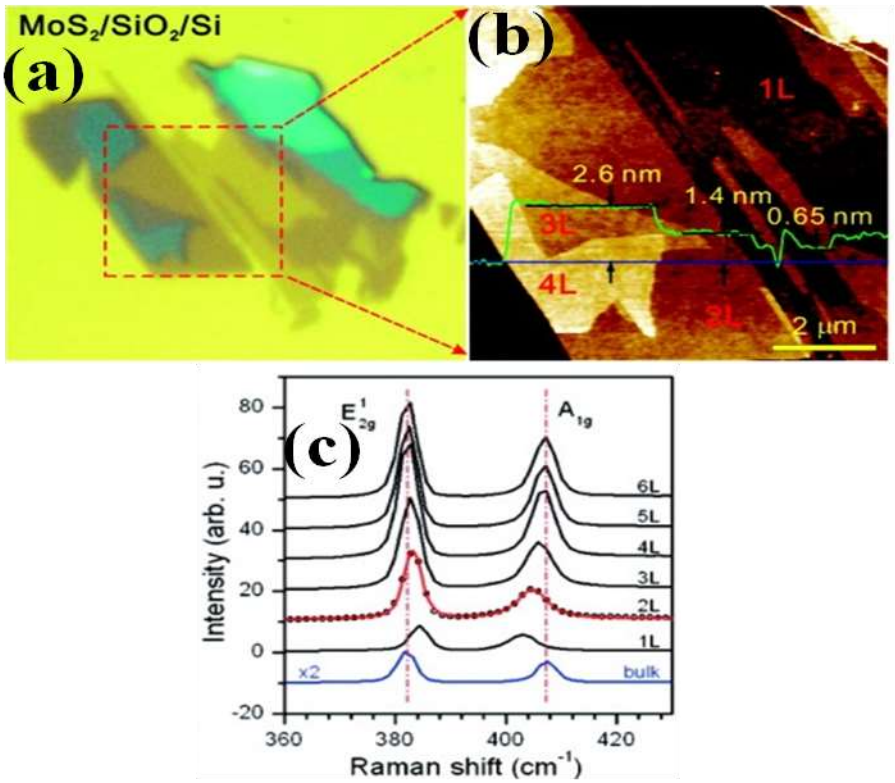


**Figure 5:** (a) Optical micrograph of thin $MoS_2$ films deposited on the $SiO_2$/Si substrate, (b) AFM height image taken for the 8×8 μm$^2$ area indicated by dotted lines in (a) and (c) Raman spectra of thin (nL) and bulk MoS2 films. The solid line for the 2L spectrum is a double Voigt fit through data (circles for 2L, solid lines for the rest). (Image taken from supporting information of ref. 65 reproduced with the permission from the American Chemical Society).

### 3.1 Physical approaches

The physical approach for the preparation of TMDCs is very simple by using mechanical exfoliation of bulk crystal using the scotch tape technique, laser irradiation or ultra-sonication etc. Significantly a lot of work has been reported on each of those techniques[150].

#### 3.1.1 Micromechanical Exfoliation method

Micromechanical Exfoliation method was first used for the preparation of Single-layer nanosheets using the scotch tape technique. This method utilizes a piece of cello tape to draw a thin film. After repeated peeling from the thin film, it is ultimately stamped onto a $SiO_2$/Si substrate and the tape is carefully removed. Significant amount of work has been done during the early stages of nanosheet preparation[151–154]. Lee *et al.*[65] reported isolation of single-and few layered $MoS_2$ films from bulk crystals of 2H-$MoS_2$ (SPI, natural molybdenite) using the micromechanical exfoliation method widely adopted for preparation of graphene samples. In a typical process, a small piece of bulk crystal $MoS_2$ was put on the sticky side of a piece of adhesive tape. This was followed by repeated folding and unfolding of the tape to produce thin flakes along the tape's surface. The tape was then pressed onto a silicon substrate covered by a 285-300 nm thick $SiO_2$ layer. After mild rubbing, the tape was removed from the substrate, leaving behind some atomically thin $MoS_2$ flakes. The size of single layers ranged from 1 to 10 μm. As can be

seen in **Figure 5**, even $MoS_2$ films of single-layer thickness provided high optical visibility on $SiO_2$/Si substrates.

**3.2 Chemical approaches**

Chemical approach is also one of the methods to exfoliate or intercalate the 2D nanomaterials by using suitable surfactants. O'Neill *et al.*[155] group has reported dispersions with significantly increased lateral nanosheet size with an increased flake size of $MoS_2$ by choosing a suitable sonication time and using an appropriate solvent. The typical procedure is as follows, $MoS_2$ concentration experiments were performed by adding the powder to 20 mL of NMP in a 100 mL capacity, flat bottomed beaker. These samples were sonicated continuously for 60 min using a horn probe sonic tip. The beaker was connected to a cooling system that allowed for cold water (5 °C) to flow around the dispersion during sonication. They were then centrifuged at 1500 rpm for 45 min. For the concentration versus sonication time experiments, 100 mL of NMP was added to 10 g of $MoS_2$. The sonic tip was pulsed for 8s on and 2s off to avoid damage to the processor and reduce solvent heating and thus degradation. During sonication, 5 mL aliquots were removed at certain time intervals and centrifuged. A TEM image of the flakes morphology is shown in **Figure 6B**. The flakes look very similar to the ones shown in **Figure 6A.** As before, most flakes are relatively thicker with a small population (10−15%) being relatively thinner (inset). On the other hand, the micro exfoliations of transition material layered dichalcogenides are also reported well in the literatures[71,126,156]. A lot of work has been carried out in the

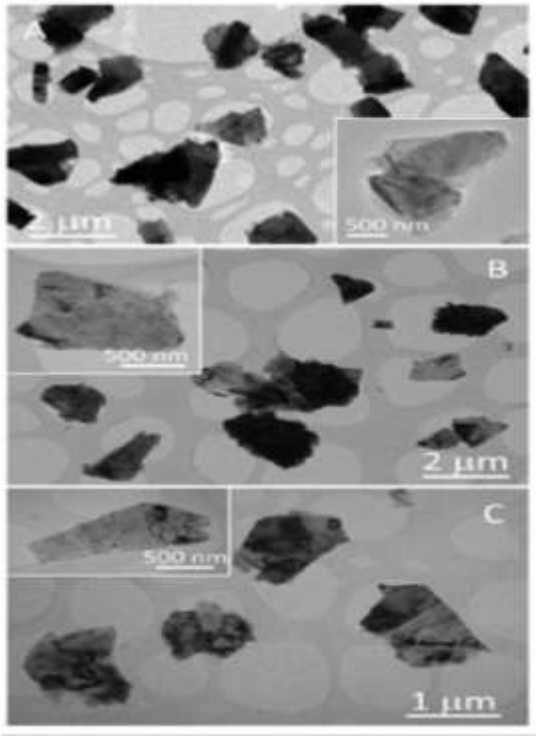


**Figure 6:** TEM micrographs of size selected dispersions of $MoS_2$ nanoflakes produced by centrifugation at 300 rpm as part of (A) the normal regime, (B) the reduced centrifugation regime, and (C) the reduced centrifugation regime followed by a 100 fold dilution in NMP. The insets show examples of thinner flakes observed in each case. (Image taken from ref. 156 reproduced by the permission from the American Chemical Society).

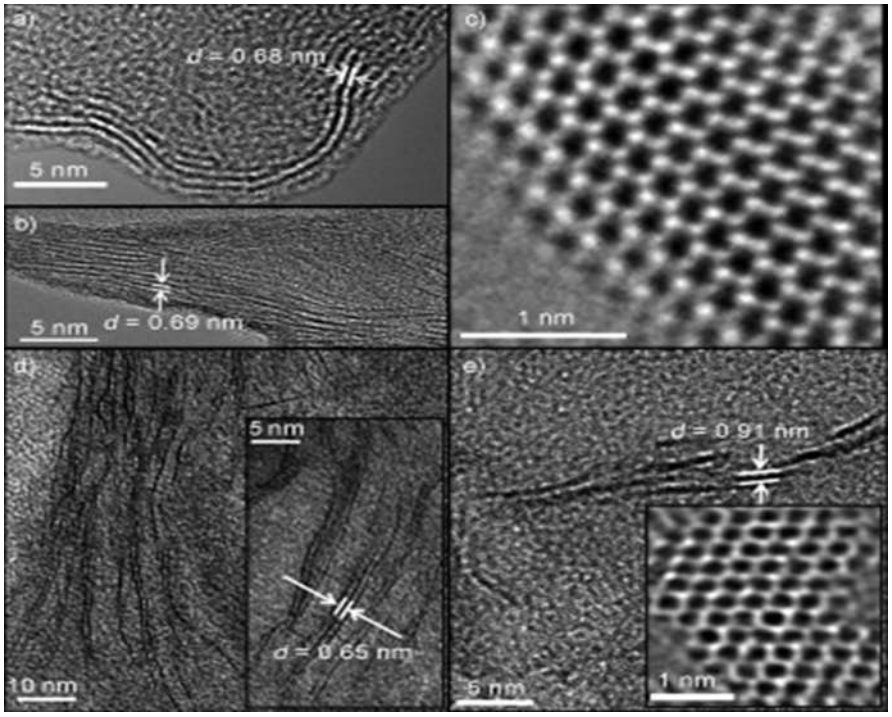


**Figure 7:** TEM images of $MoS_2$ layers obtained by Methods 2 and 3. c) High-resolution TEM image of layered $MoS_2$ from Method 3. d, e) Images of $WS_2$ layers from Methods 1 and 2, respectively. The bends in the layers may arise from defects. (Image taken from ref. 158 reproduced by the permission of Wiley).

preparation of $MoS_2$, $WS_2$ single layers by micro exfoliation method[71,131,152,156,157] for the use in various next generation nanoelectronic devices.

Though micromechanical solvent dispersion and sonochemical exfoliation produces transition metal layered dichalcogenides of the highest quality (with least defects), the method is limited by its low productivity. Chemical exfoliation, on the other hand, possesses the advantages of bulk scale production. At the same time, it has got a lot of disadvantages like being highly toxic and its contribution towards highly exothermic reactions. It includes many methods such as reduction of TMDCs by chemical vapor deposition, physical vapor deposition, hydrothermal method, microwave method etc[158–161].

### 3.2.1 Intercalation or solvent assisted exfoliations

Exfoliation in solvents is also one of the novel techniques for the preparation of single layer TMDCs as well as for the complete exfoliation of $MX_2$ sheets. This is a very simple method in which the bulk sample is thoroughly dispersed in the solvent. Matte *et al.*[157] prepared $MoS_2$ and $WS_2$ single layers by implementing various types of intercalation assisted methods. According to their procedure, the intercalation and exfoliation of $MoS_2$ and $WS_2$ were carried out in two steps. The first step was to intercalate the sulfide with lithium by soaking 100 mg of the sulfide in 10 mL of n-butyllithium in 5 mL of hexane in a nitrogen atmosphere for 72 h at 373 K. Then the intercalated samples were washed with hexane several times to remove any unreacted n-butyllithium. The intercalated sample was exfoliated by ultrasonication with distilled water in a closed vial, during which profuse evolution of gas was observed and an opaque suspension of the layered sulfide was formed. The suspension was centrifuged and the

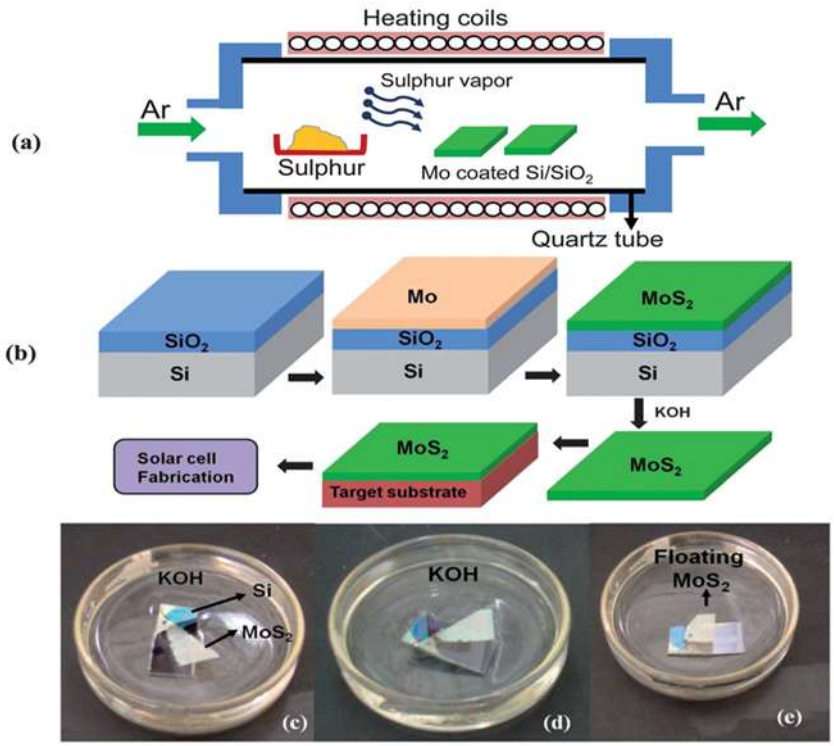


**Figure 8:** (a) Schematic of the CVD growth setup showing the reaction of sulphur vapor with Mo film pre-deposited on Si–$SiO_2$ substrate for the growth of a $MoS_2$ nanomembrane. (b) Major process steps involved in the synthesis of the $MoS_2$ nanomembrane, layer transfer, and subsequent fabrication of a Schottky-barrier solar cell. The KOH wet etching process was used to detach the $MoS_2$ nanomembrane from $SiO_2$–Si substrate. (c and d) Partially floating $MoS_2$ nanomembrane in KOH solution. (e) Free-floating $MoS_2$ nanomembrane in KOH to be transferred onto an ITO-coated glass substrate for solar cell fabrication. (Nanoscale 2012, **4**, 7399-7405 (ref. 206). Reproduced by permission of the Royal Society of Chemistry (RSC).

solid product collected for further characterization. In second method, they have used molybdic acid or tungstic acid with an excess of thiourea (molybdic acid/tungstic acid: thiourea 1:48) and heated at 773 K for 3 h under nitrogen atmosphere. After 3 h, the sample was cooled to room temperature under nitrogen atmosphere. The black product obtained was used as such for further analysis. The typical TEM image of $MoS_2$ and $WS_2$ are shown in **Figure 7**.

Jonathan N. Coleman *et al.*[162] have reported the synthesis of various layered compounds such as $MoS_2$, $WS_2$, $MoSe_2$, $MoTe_2$, $TaSe_2$, $NbSe_2$, $NiTe_2$, BN, and $Bi_2Te_3$ by using ultrasonication method and it can be efficiently dispersed in common solvents and can be deposited as individual flakes or formed into films. Electrical characterization of individual flakes shows n-type field-effect behavior characterized by mobilities of ~0.01 $cm^2$/Vs, which is rather lower than the observed value for mechanically exfoliated $MoS_2$ flakes[163–165].

### 3.2.2 Chemical Vapor Deposition (CVD)

CVD is being widely used in thin film based electronic industry as well as for the complete exfoliation of layered materials. It seems, a lot of interesting results have been obtained from the CVD for

the fabrication of layered nanomaterials[1661]. Also CVD has surged as an important method to obtain high-quality $MX_2$ films. Li *et al.*[167] works on an alternative route to large-scale $MoS_2$ and $WS_2$ inorganic fullerene-like nanostructures and nanoflowers by CVD techniques. Zhan *et al.*[168] reported synthesis of atomic-layered $MoS_2$ directly on $SiO_2$ substrates by a scalable CVD. The large-scale synthesis of an atomic-layered semiconductor directly on a dielectric layer paves the way for many facile device fabrication possibilities, expanding the important family of useful mono-layer or few-layer materials that possess exceptional properties, such as graphene and hexagonal boron nitride (h-BN). Many other works have also been reported on CVD, like chemical vapor sensing of exfoliated graphene[169], controlled synthesis of nanoflakes of $MoS_2$ by CVD[170] as shown in **Figure 8**.

Lee and co-workers have reported an alternative method for synthesizing large-area $MoS_2$ monolayer flakes using the gas-phase reaction of $MoO_3$ and S powders[161]. They conclude that, treatment of substrates with graphene-like molecules such as reduced graphene oxide, perylene-3,4,9,10-tetracarboxylic acid tetrapotassium salt (TPAS) and perylene-3,4,9,10-tetracarboxylic dianhydride (PTCDA) prior to deposition, assists in the layer growth. The reaction mechanism in their study is likely to be: $MoO_3 + x/2S \rightarrow MoO_{3-x} + x/2SO_2$ and $MoO_{3-x} + (7–x)/2S \rightarrow MoS_2 + (3\text{-}x)/2SO_2$, where $MoO_2$ during the reaction is an intermediate phase formed when $x = 1$. However, full coverage of the substrate is a challenge using this method. Lin and co-workers have shown that wafer-scale deposition can be achieved using the same chemistry, where few-layered $MoS_2$ was obtained after direct sulfurization of $MoO_3$ thin-films on sapphire substrates[171].

### 3.2.3 Hydrothermal method

Numerous works has been done on hydrothermal methods. Liu *et al.*[172] have demonstrated the preparation method of coral-like α-MnS–NC composite materials via a two-step reaction. First, the PVP-capped $(NH_4)_2Mn_2(SO_4)_3$ precursor was synthesized via a typical hydrothermal method, and then the precursor was sintered. Nitrogen-contained PVP was also used as the doped-N source. In a typical procedure, 0.015 mol $MnSO_4·H_2O$, an appropriate amount of $(NH_4)_2S_4O_8$, and PVP were dissolved into distilled water to form a homogeneous solution under vigorous stirring. Then the solution was transferred into a Teflon-lined stainless steel autoclave and kept in an oven at 120 °C for 2–12 h. After reaction, the products were collected by centrifugation, washed thoroughly with deionized water and ethanol, and dried at 80 °C. The as-prepared precursors were sintered in $N_2$ at different temperatures for the appropriate time. The resulting precursors and the final products were marked as HMS-t-P and HMS-t-T, respectively, where t represents hydrothermal reaction time and T, the final sintering temperature. For example, HMS-2-P is the precursor hydrothermally prepared at 120 °C for 2 h, and HMS-2-800 is the final product obtained by sintering HMS-2-P at 800 °C for 2 h. Subsequently, Wang *et al.*[173] have reported an enhanced lithium storage performances of hierarchical hollow $MoS_2$ nanoparticles assembled from nanosheets by a hydrothermal route in which 0.865 g of molybdenum trioxide powder, 0.515 g of sodium fluoride and 1.930 g of potassium thiocyanate were added to a mixture of 30 mL of distilled water and 10 mL of ethanol. After being stirred for 10 min, the solution was then transferred into a Teflon-lined stainless steel autoclave with a capacity of 50 mL. The autoclave was sealed and maintained at 200 °C for 16 h. The dark precipitates were collected and washed with dilute acid and absolute ethanol several times. Finally, the product was dried under vacuum at 60 °C. To evaluate the performances of these hierarchical hollow nanoparticles in LIBs, the solid $MoS_2$ nanoparticles were prepared by the similar procedure, using glycerine for the solvent mixture rather than ethanol. The other experiment parameters were kept as the

same. Thripuranthaka *et al.*[118] have prepared high quality few layer $MoS_2$ and $WS_2$ nanosheets at 200 $^0$C and 265 $^0$C, respectively.

### 3.2.5 Microwave irradiation

Microwave irradiation (MWI) has been demonstrated for the synthesis of a variety of nanomaterials including metals, metal oxides, bimetallic alloys and semiconductors with controlled size and shape without the need for high temperature or high pressure. MWI has also been used for the

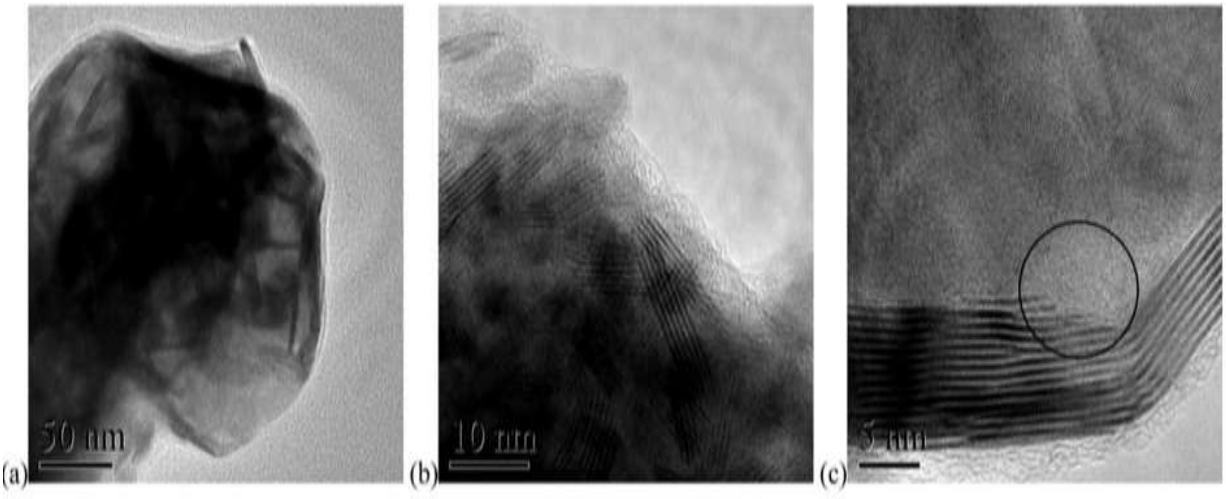


**Figure 9:** High resolution TEM images of $MoSe_2$ nanorods by Microwave Method. (Image taken from ref. 175 *J Mater Chem.* 2003, **13**, 2603-2606. Reproduced by permission of the Royal Society of Chemistry (RSC).

synthesis of TMDCs derivatives and for the exfoliation of $MX_2$ intercalation compounds. The main advantage of MWI over other conventional heating methods is heating the reaction mixture uniformly and rapidly. Due to the difference in the solvent and reactant dielectric constants, selective dielectric heating can provide significant enhancement in the transfer of energy directly to the reactants which causes an instantaneous rise in the internal temperature. The method reported here allows the rapid chemical synthesis of single layered $MX_2$.[174] Stoichiometric quantities of $Mo(CO)_6$ and Se powder were put in ethylene glycol. The system was purged for a few minutes with nitrogen prior to switching on the microwave reactor. The reactions were conducted for 1 hour under nitrogen. In the post-reaction treatment, the product was centrifuged once with the mother liquid, and a few times with ethanol, at 20 °C and 9000 rpm. The product was then dried overnight in vacuum. They have also tried other routes such as reacting a mixture of ammonium molybdate and molybdenum acetate dimer with Se in ethylene glycol to get $MoSe_2$ which is depicted in TEM images shown in F**igure 9**.

There are few recent reports[175–177] for the supercapacitor applications. Controlled, defect-guided, metal-nanoparticle incorporation onto $MX_2$ via chemical and microwave routes: electrical, thermal, and structural properties were reported by Sreeprasad *et al.*[178]

## 4. Energy applications of TMDCs.

The wide range of applications of TMDCs layered semiconductor materials for energy.

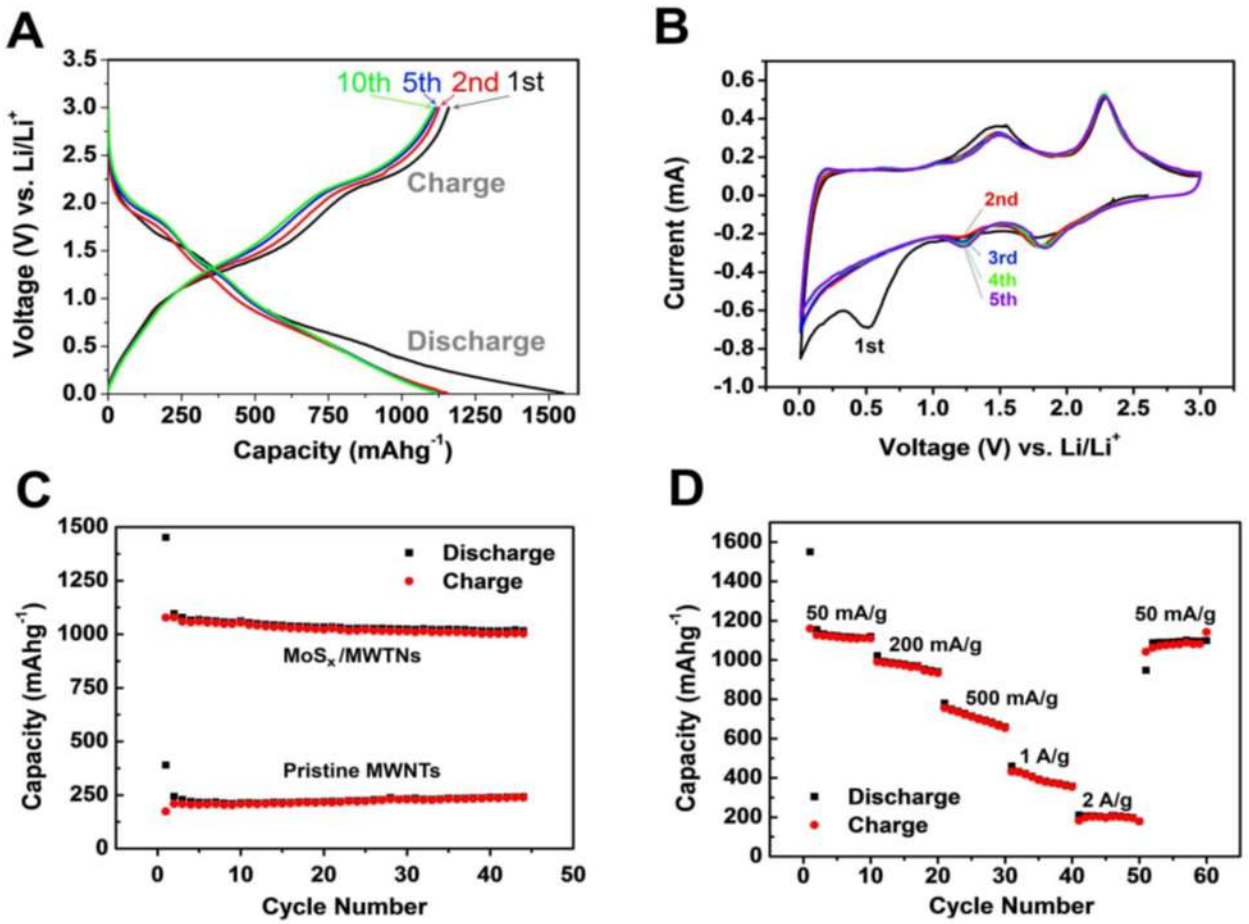


Figure 10: (A) Voltage profiles of MoSx/MWNTs charged-discharged at 50 mA g21, (B) Representative cyclic voltammograms of MoSx/MWNTs composite for the first 5 cycles at a scan rate of 0.5 $mVs^{-1}$ between 0.01 V and 3 V. (C) comparison of cycling stability between MoSx/MWNTs and MWNTs charged-discharged at 50 mA $g^{-1}$), and (D) Rate capability of MoSx/MWNTs charged and discharged at various current densities. (Image taken from ref. 186, reproduced by the permission of Nature publishing group).

**4.1 Supercapacitors**

Supercapacitors have become promising candidates for next generation high-performance power devices because of their high power density, fast power delivery or uptake and excellent cycle-to-cycle stability[179–183]. It can store charges in a highly reversible pathway. Also the storage of electrochemical energy in battery, "supercapacitor," and double-layer capacitor devices is considered. Supercapacitors can be classified into two groups, one is the electric double layer capacitor (EDLC), which stores energy through the charge accumulation at the electrode–electrolyte interface/Helmholtz layers via induced polarization. The other type is the pseudo-capacitor, whose working principle is based on rapid charge transfer through redox reaction. TMDCs layers can facilitate electron transport through $MX_2$ nanostructures, which provides easier and faster ion diffusion between $MX_2$ layers/electrolytes and produces high values of specific capacitance[184]. For example, $MoS_2$ nanosheets possess a large specific surface area and interlayer space for the ion intercalation and have a wide range of oxidation states from $Mo^{2+}$ to $Mo^{6+}$ in the redox reaction. Therefore, its use as a combined double-layer capacitor and pseudo-

capacitor is highly expected. The resulting supercapacitor can provide both the double-layer and faradaic capacitance/pseudo capacitance and is able to function at alternating current frequencies up to 100 Hz. Since the thickness of $MoS_2$ nanosheets is up to 100 nm, it is anticipated that reduction of the nanowall thickness to few-layer or single-layer would enlarge the specific surface area of the electrode material, and thus provide larger capacitance. It also attracts prime attention as an auxiliary power source to secondary batteries because of fast charging/discharging capability, high power density, and excellent cyclability as shown in **Figure 10.**[185]

Recent studies demonstrate that $MoS_2$ nanosheets prepared by hydrothermal method and by exfoliation act as a promising typical pseudocapacitive material for supercapacitor application[184,186]. Having advantages of high conductivity and high surface area, metallic $VS_2$ nanosheets have been employed to fabricate in plane supercapacitor electrodes[187]. Since the storage of electrical energy by the supercapacitor occurs near the interface between electrode and electrolyte, the optimization of the surface structure of electrode materials is very crucial in improving the energy storage capacity of supercapacitors. The hybridization with the exfoliated 2D nanosheets is effective in exploring highly efficient electrode materials for supercapacitors since the 2D nanosheet-based nanohybrids possess highly porous structure with expanded surface area. Furthermore, the sub-nanometer level thickness of the exfoliated 2D nanosheets makes possible an optimization of the power density of 2D nanosheet-based hybrid materials via a strong electronic coupling with hybridized conductive materials.[188–197]

Because of the unique microstructure with combination of two 2D materials and having high surface area due to their novel crystal structure, TMDCs/graphene hybrids have a potential to significantly enhance the electrochemical performance as supercapacitor electrodes[193,198–200]. The success of applying a homo or heterogeneous nanostructured hybrid materials for supercapacitors, strongly depends on the factors such as: employment of proper synthesis methods to prepare the desired nanostructure; selection of a proper combination of different materials; designation and optimization of the heterogeneous nanostructure[193,198–200]. In the TMDCs/graphene hybrids, the large surface area and the nanoscale size of $WS_2$ and graphene greatly reduce the diffusion length over which both ions and electrons must transfer during the charge-discharge process. Graphene helps to enhance the conductivity of the hybrids if there is uniform coverage of TMDCs on graphene and it facilitates fast transportation of electrons throughout the hybrid electrode material. Also the heterojunctions with conductive network effectively prevents the volume expansion/contraction and aggregation of electroactive materials during charging-discharging process and improves the long cycle performance of the supercapacitors[193,198].

### 4.2 Solar Cells

The demand of solar cells can be experienced from the following current status of power consumption worldwide. At present, consumption of power is about 13 terawatts (TW) worldwide. So far, only about 5 GW of power is generated from solar energy by solar cells[19,201–207]. From the literature, it has been realized that the 2D graphene, 2D metal dichalcogenides and their nanocomposites have great potentials to replace the solar cells made from silicon that are currently being used. The majority of solar cells on the market are single-junction silicon wafer devices including single crystal and multicrystalline silicon, which are known as first generation solar cells[208–210]. Their main drawback is associated with their indirect optical band gap that requires a thick active layer for the solar conversion and thus costly fabrication of large area materials. Furthermore, these cells suffer from many efficiency losses for energy conversion, such as “red losses” (photons with energies below the band gap of the device cannot be absorbed) and “blue losses” (photons with energies above the band gap lose their excess energy as

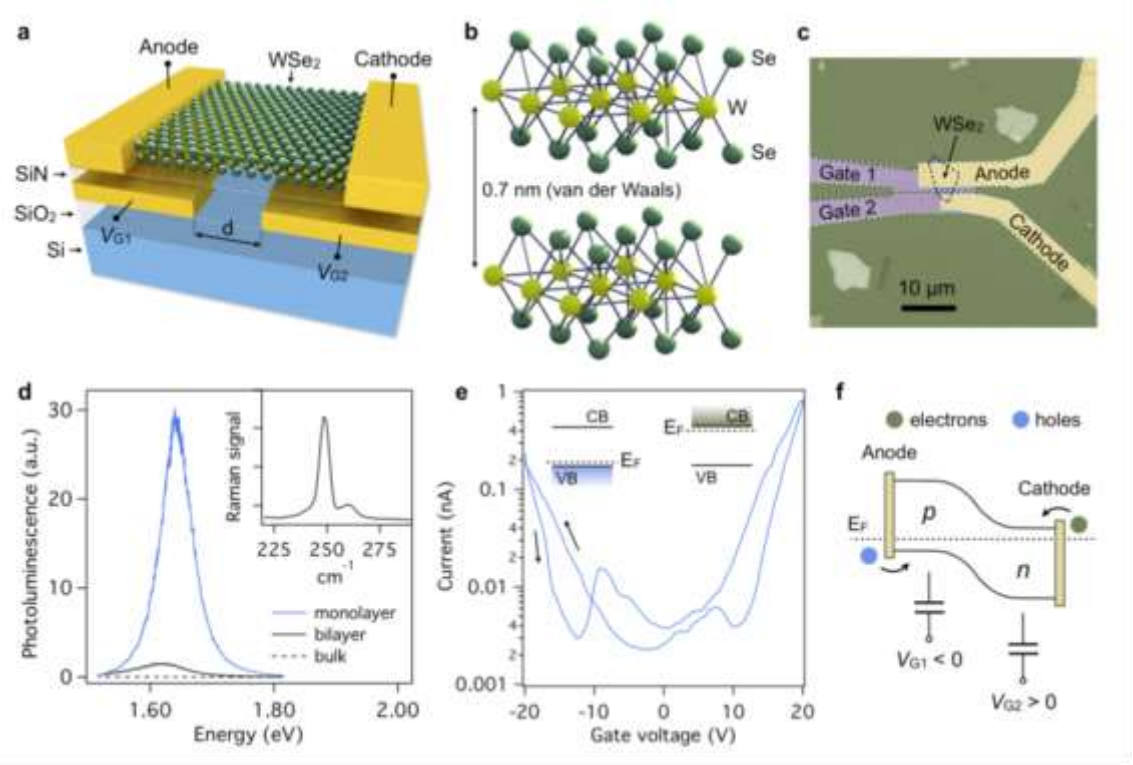


**Figure 11:** Solar cell device of $WSe_2$ (a) Schematic drawing of the device structure. (b) Three-dimensional schematic representation of $WSe_2$. Monolayers are ≈0.7 nm thick and are mechanically exfoliated from a bulk crystal. (c) Colored microscope image of the device. In between the gates electrodes and the $WSe_2$ flake there is a 100-nm-thick gate dielectric. The anode electrode is made of Pd/Au and the cathode of Ti/Au. The gap between the gates is 460 nm wide. (d) PL from mono- (solid blue line), bi- (solid black line), and multi-layer (dashed black line) $WSe_2$ flakes on $SiO_2$. Inset: Raman spectrum of a monolayer. (e) Gate characteristic of the device. Both electrons and holes can be injected into the channel. The curve was obtained by scanning the gate voltage from -20 V to 20 V and back. (f) Band diagram when operated as p-n junction diode ($V_{G1} < 0$, $V_{G2} > 0$). Asymmetric contact metallization allows more efficient electron (green) and hole (blue) injection. (Image taken from ref. 8 is reproduced by the permission of Nature publishing group).

heat)[211–213]. TMDCs are a rapidly rising phenomenon in areas like material sciences and nanotechnology. This two dimensional material exhibits unique properties, such as low resistance, excellent optical transmittance, and high mechanical and chemical stabilities. These exceptional advantages possess great promise for its potential applications in photovoltaic devices. The electronic band structures of semiconductors directly influence their ability to absorb and emit light. As the TMDCs are already known for their flexible band gaps depending upon the varying number of layers, they can effectively be employed as the possible candidates for the fabrication of new generation solar cells, making use of their thickness monitored photoactivity[214]. The semiconducting monosulfide and disulfide ($S_2$) nanomaterials exhibit van der Waals bonding, crystallizes in a layer-type structure and is of interest as an absorber layer for thin-film solar cells. This can be attributed to the generation of recombination centers, especially sulfur vacancies during the ion bombardment of the films due to the low defect-formation energy of disulfide, an intrinsic property of transition metal dichalcogenides. $WS_2$ is a semiconducting sulfide that

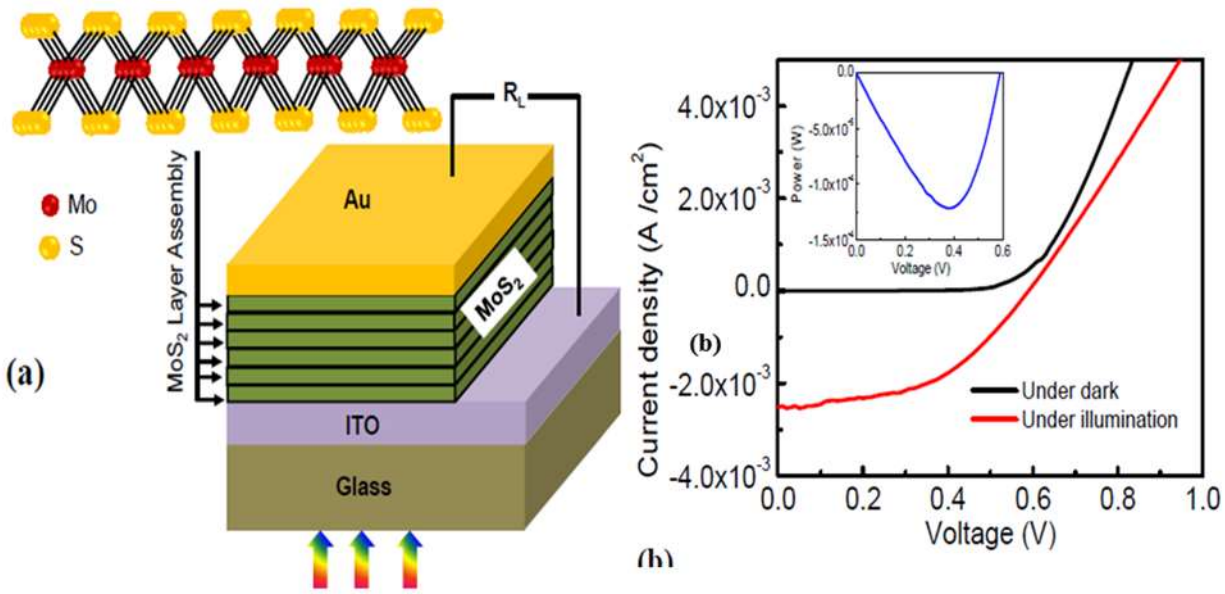


**Figure 12:** (a) Schematic of solar cell structure showing stack of $MoS_2$ nanomembranes on ITO substrate with Au contact.(b) Measured dark & illuminated J – V of solar cells with a stack of $MoS_2$ nanomembranes having thickness of ~10 nm.( Image taken from ref. 179. Nanoscale 2012, **4**, 7399-7405. Reproduced by permission of The Royal Society of Chemistry (RSC).

crystallizes in a layer-type structure similar to that of the well-known layer-type materials, graphite or mica. It belongs to the class of transition-metal dichalcogenides (TMDCs) like $MoS(Se)_2$ and $WSe_2$, which are all semiconductors and of great interest as absorbers for thin-film solar cells as shown in **Figure 11**.

This is caused by its well-defined bandgaps which falls within the range of 1–2 eV and the extraordinarily high absorption coefficients, exceeding 105 $cm^{-1}$. The TMDCs crystallize in the molybdenite structure ($P6_3/mmc$, no. 194), where the metal atoms are arranged in close packed hexagonal layers. The anisotropic bonding of these materials leads to strongly anisotropic electrical and mechanical properties, which can be used advantageously. Yun *et al.*[214] reported on work-function of $MoS_2$ interfacial layers which can be efficiently modulated by p-doping and n-doping treatments. J.J. Devadasan *et al.*[215] have reported p-$WS_2$ thin film based PEC solar cells. They deposited thin films of $WS_2$ on CTO coated glass substrate by electrodeposition technique and studied its photochemical properties which showed promising results. So $WS_2$ readily stands as an active material for the fabrication of solar cells. The major drawback with the photovoltaic application of TMDCs lies in separating the photogenerated electron-hole pairs in an efficient way. However, Britnell *et al.*[216] have demonstrated a possible solution by stacking photoactive TMDC layer in between two graphene layers (which act as transparent electrodes) and doping the two graphene layers as such to position Fermi level and to enable photocurrent extraction. Their method can be used for other TMDCs as well. Their device showed an enhanced photoresponsivity which was above 0.1 A/W and a quantum efficiency of above 30%. Due to the fact that the TMDCs nanosheets boast some intriguing physical as well as chemical characteristics such as high surface area, low catalyst load, good electrical conductivity and chemical stability, they readily pose an alternative as well as competitive solution to commercial carbon black as catalyst support. It has already been reported that

$WSe_2$ shows a promising conversion efficiency of about 12.4% due to its high photoactivity property under suitable conditions. Shanmugam *et al.*[206] have shown that stacked layer of $MoS_2$ (**Figure 12**) fabricated by chemical vapor deposition method using indium tin oxide (ITO) as the substrate shows potential results to be used as an efficient solar cell material.

Furthermore, in their conducive report, S.M. *Delphine et al.*[217] have also explained that if the effective surfaces of $WSe_2$ crystals were treated with aqua regia then the solar to electric conversion efficiency would reach up to 14%. Further improvement in the efficiency (~17%) of $WSe_2$ crystals were observed in polyiodide solution which was used as an electrolyte. Similar effects have been observed in case of $MoSe_2$ crystals too[218]. The cleaving process affects the active edges of both $WSe_2$ as well as $MoSe_2$ and enhances their photovoltaic properties resulting in higher conversion efficiency. Both the TMDC materials show higher stability and resistance towards photocorrosion as compared to other organic solar cells[218]. Many of the recent reports have shown that transition metal dichalcogenides and their hybrids can be synthesized in a very cost effective way and have the ability to actively absorb much more radiated energy from the solar energy spectra as compared to the conventional solar cells made from both organic materials as well as silicon[219–221]. Furthermore, the relative thickness of the fabricated devices using TMDCs would be much less, bringing in the possibility for transparent, light weight and flexible solar cells. The importance of harvesting solar energy is obvious because it only can meet up to the huge demand of power arising all over the world (~30 TW) though other renewable energy sources would definitely play their part. Also the emerging field comprising of the 2D layered TMDCs is providing an ideal platform to harvest the enormous energy provided by the sun in a way which is both renewable and cost effective.

**4.3 Lithium Ion batteries**

The Li-ion battery (LIB) has been considered as one of the most promising energy storage systems, because of its high absolute potential against the standard hydrogen cell (-3.04 V) and its low atomic weight (M = 6.94 $gmol^{-1}$), leading to the large energy density with a theoretical value of up to 400 W h $kg^{-1}$. Layered bulk crystals such as graphite and metal dichalcogenides (e.g. $TiS_2$) are traditional insertion-type electrode materials for LIBs[113]. The massive production of single- and multi-layer $MoS_2$ nanosheets from the top-down solution-phase exfoliation or the bottom-up chemical synthesis may enable their widespread application for batteries. Recently, restacked $MoS_2$ nanosheets prepared from chemical lithiation and exfoliation have been fabricated into electrodes for LIBs and compared with electrodes made from the bulk $MoS_2$. It was found that the charge capacity of the bulk $MoS_2$ decreased from over 800 mA h $g^{-1}$ to 226 mA h $g^{-1}$ after 50 cycles, whereas the restacked $MoS_2$ showed much better cycling stability and retained a high capacity of 750 mA h $g^{-1}$ after 50 cycles[222]. The restacked $MoS_2$ nanosheets possessed an enlarged inter-sheet spacing compared to the raw $MoS_2$, which lowered the barrier for Li-intercalation to give the better ionic conductivity[222,223]. Layered nanomaterials and its derivatives can be hybridized with other electrochemical active materials to form composite electrodes for LIBs, where the graphene sheets can provide conductive paths, enlarge effective surface area, and improve the cycling stability of the electrodes. Recently, Chang and Chen[223] prepared few-layer $MoS_2$ and reduced graphene oxide (rGO) hybrids via the L-cysteine-assisted hydrothermal process, and then used them for LIBs. The high practical capacities and fast Li ion movement in TMS originate from two main reasons with respect to the mechanism of Li ion storage. The weak van der Waals bounded layer structure (S-metal-S) can induce easy intercalation/deintercalation of Li ions, lowering the energy barrier for Li ion movement and the transition metal compound can store a large number of Li ions through a conversion reaction.

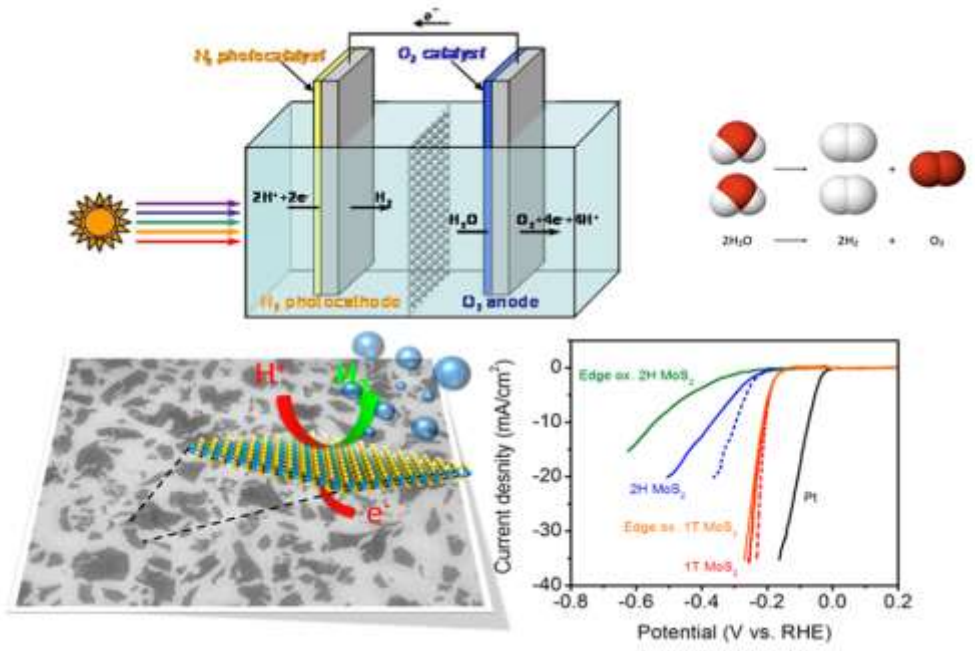


**Figure 13:** $MoS_2$ Nanosheets as Catalysts for Hydrogen Evolution Reaction (Image taken from ref.232 is reproduced by the permission of the American Chemical Society).

However, the poor cyclic stability hinders their use as the alternative anode material for LIBs and it occurs due to the large volume change during the charge/discharge process, which causes pulverization of electrodes and thus deteriorates anode performance. Moreover, the graphene assisted $MoS_2$ compounds only yielded a 250 mAh $g^{-1}$ specific capacity at a 10000 mA $g^{-1}$ discharging rate, which is also an insufficient rate capability for commercialization. These atomically thin layers of $MoS_2$ display enhanced electrical and optical properties due to the quantum confinement effect. Although the first measurements of carrier mobility in atomically thin layers of $MoS_2$ resulted in the observation of relatively small values in the range of 0.5–3.0 $cm^2$ $V^{-1}s^{-1}$. Balendhran *et al.*[103] have demonstrated the successful synthesis of layered hexagonal $MoS_2$, through a simple method of thermal evaporation in a reduction environment. This method uses temperatures less than 830 °C which is much less than the temperature, which is required for the direct evaporation of $MoS_2$. By the application of the mechanical exfoliation technique on the layered $MoS_2$, we have obtained atomically thin layers of $MoS_2$ with the steps of ~0.65 nm corresponding to the fundamental thickness of the material. These atomically thin layers can be utilized in the fabrication of electronic devices of high carrier mobility to pave the way into the next generation of electronic devices especially Lithium ion batteries[223–227]. $WS_2$, whose physical and chemical properties are more or less similar to that of $MoS_2$, also has been studied extensively as an active material for its possible application in the fabrication of LIBs. The electrochemical properties of superacid-treated $WS_2$ have been carefully observed in a Li-ion half-cell configuration. It showed an impressive specific capacity of 470 mAh/g at 25 A/g of current discharge rate[20]. The superacid-treated $WS_2$ showed much enhanced electrochemical properties than that of pristine $WS_2$ and the enhancement factor is contributed by the increased intercalation of Li ions between the cleaved superacid-treated $WS_2$ layers. In another study[228], it has been theoretically calculated that Vandium disulfide ($VS_2$) also shows high specific capacity of about ~466mAh/g and in comparison to $MoS_2$ and $WS_2$, have lower/similar Li ion diffusion barrier and low

average open circuit voltage of 0.93 V (vs $Li/Li^+$). The flexibility with which the layers of TMDCs can be modified/stacked and the easy intercalation/deintercalation of ions through those layers, makes the TMDCs much more impelling in the area of fabricating nanoscale devices having the ability to show ultra-high energy storage/delivering capacity.

**4.4 Water Splitting**

Besides solar energy, water has the potential to provide clean energy without any kind of contribution towards environmental issues. The main purpose is to breakdown the hydrogen part and makes use of $H_2$ as a clean source of energy. Many methods have been employed to efficiently carry out the splitting of water into hydrogen ($H_2$) and oxygen (O). Currently used catalysts of Pt-group metals are highly efficient in carrying out the hydrogen evolution reaction (HER) but which is too expensive and thus may not be used for the mass production of hydrogen. There are reports in which it has been claimed that promising alternatives are actually available[229–231]. Water splitting is the general term for a chemical reaction in which water is separated into oxygen and hydrogen[224,232–237]. Till date, TMDCs in their bulk form have not been very efficient in HER, and were being widely used to enhance the concentration of catalytically active edges as shown in **Figure 13**.

The use of earth-abundant electrocatalysts would significantly reduce the high cost associated with currently used Pt-group electrocatalysts. Among TMDCs, $MoS_2$ and $WS_2$, which are widely available in the earth's crust, show improved performance concerning HER. However the major setback is their application in bulk form and to produce hydrogen on a large scale. Recent report explains how monolayered nanosheets of chemically exfoliated $WS_2$ can become an interesting candidate for carrying out the HER efficiently with having very low overpotentials[230]. Furthermore, A detailed computational study has been performed by Zhuang and Hennig in which they have made use of first-principles design approach for 2D metal dichalcogenides, $MX_2$ (M = Nb, Mo, Ta, W, Ti, V, Zr, Hf and Pt; X = S, Se, and Te)[238]. They have found that these TMDCs are ideal for being functionalized as photocatalysts in order to carry out the water splitting process much efficiently. According to their data, $MoS_2$, $WS_2$, $PtS_2$ and $PtSe_2$ are highly active photocatalysts in comparison to other TMDCs. Density functional theory calculations have also indicated that the edges of $MoS_2$ nanosheets are active for HER. The HER activity of various catalysts can be summarized in the 'volcano plot', where the exchange current density for different catalytic metals in acids is plotted as a function of the DFT-calculated metal–hydrogen bond strength. Layered TMDCs has received much attention. Zhang and colleagues have become pioneers in the field of TMDCs exfoliation by lithiation for electrochemical reactions. They reported the catalytic activity of 2D $MoS_2$ nanosheets and metal nanoparticle (Pt, Pd, and Ag) decorated $MoS_2$ sheets, and found that the metal nanoparticles had mainly (111) and (101) orientations on the $MoS_2$ surface. In addition, The $MoS_2$ sheets gave a Tafel slope of 94mV/dec, and Pt-$MoS_2$ hybrid sheets showed much higher electrocatalytic activity (Tafel slope of 40mV/dec) towards the HER. Recently, we were able to synthesize $WS_2$ and $WS_2$/rGO hybrid sheets via a hydrothermal method. The 2H-$WS_2$ grown on the rGO interconnected conducting network was able to afford rapid electron transport and improved crystallinity after annealing, inducing increased catalytic activity. Therefore, the hybrid material showed excellent HER activity with a small overpotential, and a Tafel slope of 58mV/dec. HER performance of a variety of $MoS_2$ and $WS_2$ structures to enhancing the HER performance of $MoS_2$ and $WS_2$, 2D $MoS_2$/$WS_2$ sheets and their hybrids are identified as being highly promising candidates to replace conventional Pt catalysts. However, many challenging issues associated with the use of these materials remain, and will form the basis of future research themes. The most important issue that requires elucidation is the exact mechanisms by which the

HER proceeds on $WS_2$ and $MoS_2$, as it is known that they vary with materials. Further details on the mechanism need to include crystallinity and identification of active sites and the effect of strain in the 1T phase on HER performance should be clarified[231,232,234,236–249]. The knowledge gained then needs to be successfully transferred to the development of new TMDCs structures or engineered surfaces for maximizing HER performance. In addition, hybrid materials such as $WS_2$/rGO hybrid sheets have demonstrated great promise for overcoming some of the limitations of TMDs, and for affording new functions for efficient $H_2$ evolution.

## CONCLUSIONS AND OUTLOOK:

Considerable advancement has been made in many application areas of inorganic semiconducting layered materials. The effort has focused on use of single sheet & few layer thick sheet device fabrications such as solar cell, Li ion battery, water splitting so that the available renewable sources of energy could be successfully exploited to the benefit of humankind. This fundamental knowledge has begun to translate into real applications although combination issues such as complementary doping and nanocomposite of inorganic layered materials with graphene require more effort. Similarly, access to high-quality, large-area inorganic single-layers and few layers for specific application is emerging with the advent of various synthesis approaches though there are still some issues/constraints which are yet to be addressed completely. These devices would surely bring a revolutionary change to the current scenario of depletion in naturally available non-renewable energy sources for a sustainable future for next generations. Also for making the devices to be commercialized, it is important for the devices to have some basic properties like flexibility, stretchability, and/or transparency. Indubitably, the future of layered TMDs based energy related materials must be very intense and stimulating.

## ACKNOWLEDGEMENTS

The authors would like to thank Prof. C. N. R. Rao, FRS (ICMS & JNCASR Bangalore), Prof. Vinayak P. Dravid (Northwestern University, USA), for constant support and encouragement. One of the authors, Dr. D. J. Late, would like to thank DST (Government of India) for Ramanujan fellowship (SR/S2/RJN-130/2012). Partial support by DST Fast-Track project (SB/FT/CS-116/2013) and CSIR-NCL MLP 028626 are gratefully acknowledged.

## REFRENCES:

[1] Baxter, J.; Bian, Z.; Chen, G.; Danielson, D.; Dresselhaus, M. S.; Fedorov, A. G.; Fisher, T. S.; Jones, C. W.; Maginn, E.; Kortshagen, U.; et al. Nanoscale Design to Enable the Revolution in Renewable Energy. *Energy Environ. Sci.* **2009**, *2*, 559–588.

[2] Dubacheva, G. V; Liang, C.-K.; Bassani, D. M. Functional Monolayers from Carbon Nanostructures – Fullerenes, Carbon Nanotubes, and Graphene – as Novel Materials for Solar Energy Conversion. *Coord. Chem. Rev.* **2012**, *256*, 2628–2639.

[3] Lightcap, I. V; Kamat, P. V. Graphitic Design: Prospects of Graphene-Based Nanocomposites for Solar Energy Conversion, Storage, and Sensing. *Acc. Chem. Res.* **2012**, *46*, 2235–2243.

[4] Wei, L.; Yushin, G. Nanostructured Activated Carbons from Natural Precursors for Electrical Double Layer Capacitors. *Nano Energy* **2012**, *1*, 552–565.

[5] Das, S.; Prakash, A.; Salazar, R.; Appenzeller, J. Toward Low-Power Electronics: Tunneling Phenomena in Transition Metal Dichalcogenides. *ACS Nano* **2014**, *8*, 1681–1689.

[6] Lv, R.; Robinson, J. A.; Schaak, R. E.; Sun, D.; Sun, Y.; Mallouk, T. E.; Terrones, M. Transition Metal Dichalcogenides and Beyond: Synthesis, Properties, and Applications of Single- and Few-Layer Nanosheets. *Acc. Chem. Res.* **2014**, *48*, 56–64.

[7] Pospischil, A.; Furchi, M. M.; Mueller, T. Solar-Energy Conversion and Light Emission in an Atomic Monolayer P-N Diode. *Nat Nano* **2014**, *9*, 257–261.

[8] Rao, C. N. R.; Matte, H. S. S. R.; Subrahmanyam, K. S.; Maitra, U. Unusual Magnetic Properties of Graphene and Related Materials. *Chem. Sci.* **2012**, *3*, 45–52.

[9] Ogawa, S. Magnetic Properties of 3d Transition-Metal Dichalcogenides with the Pyrite Structure. *J. Appl. Phys.* **1979**, *50*, 2308–2311.

[10] Zhou, Y.; Yang, C.; Xiang, X.; Zu, X. Remarkable Magnetism and Ferromagnetic Coupling in Semi-Sulfuretted Transition-Metal Dichalcogenides. *Phys. Chem. Chem. Phys.* **2013**, *15*, 14202–14209.

[11] Pumera, M.; Sofer, Z.; Ambrosi, A. Layered Transition Metal Dichalcogenides for Electrochemical Energy Generation and Storage. *J. Mater. Chem. A* **2014**, *2*, 8981–8987.

[12] Tributsch, H. Photoelectrochemical Behaviour of Layer-Type Transition Metal Dichalcogenides. *Faraday Discuss. Chem. Soc.* **1980**, *70*, 189–205.

[13] Chhowalla, M.; Shin, H. S.; Eda, G.; Li, L.-J.; Loh, K. P.; Zhang, H. The Chemistry of Two-Dimensional Layered Transition Metal Dichalcogenide Nanosheets. *Nat Chem* **2013**, *5*, 263–275.

[14] Wang, H.; Feng, H.; Li, J. Graphene and Graphene-like Layered Transition Metal Dichalcogenides in Energy Conversion and Storage. *Small* **2014**, *10*, 2165–2181.

[15] Huang, K.-J.; Wang, L.; Liu, Y.-J.; Wang, H.-B.; Liu, Y.-M.; Wang, L.-L. Synthesis of polyaniline/2-Dimensional Graphene Analog $MoS_2$ Composites for High-Performance Supercapacitor. *Electrochim. Acta* **2013**, *109*, 587–594.

[16] Muller, G. A.; Cook, J.; Kim, H. S.; Tolbert, S. H.; Dunn, B. High Performance Pseudocapacitor Based on 2D Layered Metal Chalcogenide Nanocrystals. *Nano Lett.* **2015**.

[17] Ellmer, K. Preparation Routes Based on Magnetron Sputtering for Tungsten Disulfide ($WS_2$) Films for Thin-Film Solar Cells. *Phys. status solidi* **2008**, *245*, 1745–1760.

[18] Tributsch, H. The MoSe 2 Electrochemical Solar Cell: Anodic Coupling of Electron Transfer to D → D Photo-Transitions in Layer Crystals. *Berichte der Bunsengesellschaft für Phys. Chemie* **1978**, *82*, 169–174.

[19] Shanmugam, M.; Bansal, T.; Durcan, C. A.; Yu, B. Molybdenum Disulphide/titanium Dioxide Nanocomposite-Poly 3-Hexylthiophene Bulk Heterojunction Solar Cell. *Appl. Phys. Lett.* **2012**, *100*, 153901.

[20] Bhandavat, R.; David, L.; Singh, G. Synthesis of Surface-Functionalized $WS_2$ Nanosheets and Performance as Li-Ion Battery Anodes. *J. Phys. Chem. Lett.* **2012**, *3*, 1523–1530.

[21] Xiao, J.; Choi, D.; Cosimbescu, L.; Koech, P.; Liu, J.; Lemmon, J. P. Exfoliated $MoS_2$ Nanocomposite as an Anode Material for Lithium Ion Batteries. *Chem. Mater.* **2010**, *22*, 4522–4524.

[22] Kong, D.; Cha, J. J.; Wang, H.; Lee, H. R.; Cui, Y. First-Row Transition Metal Dichalcogenide Catalysts for Hydrogen Evolution Reaction. *Energy Environ. Sci.* **2013**, *6*, 3553–3558.

[23] Chen, T.-Y.; Chang, Y.-H.; Hsu, C.-L.; Wei, K.-H.; Chiang, C.-Y.; Li, L.-J. Comparative Study on $MoS_2$ and $WS_2$ for Electrocatalytic Water Splitting. *Int. J. Hydrogen Energy* **2013**, *38*, 12302–12309.

[24] Du, F.; Yu, D.; Dai, L.; Ganguli, S.; Varshney, V.; Roy, A. K. Preparation of Tunable 3D Pillared Carbon Nanotube–Graphene Networks for High-Performance Capacitance. *Chem. Mater.* **2011**, *23*, 4810–4816.

[25] Civalek, Ö. Elastic Buckling Behavior of Skew Shaped Single-Layer Graphene Sheets. *Thin Solid Films* **2014**, *550*, 450–458.

[26] Diggikar, R. S.; Late, D. J.; Kale, B. B. Unusual Morphologies of Reduced Graphene Oxide and Polyaniline Nanofibers-Reduced Graphene Oxide Composites for High Performance Supercapacitor Applications. *RSC Adv.* **2014**, *4*, 22551–22560.

[27] Geim, A. K. Graphene: Status and Prospects. *Sci.* **2009**, *324* , 1530–1534.

[28] Geim, A. K.; Novoselov, K. S. The Rise of Graphene. *Nat Mater* **2007**, *6*, 183–191.

[29] Ghosh, A.; Late, D. J.; Panchakarla, L. S.; Govindaraj, A.; Rao, C. N. R. $NO_2$ and Humidity Sensing Characteristics of Few-Layer Graphenes. *J. Exp. Nanosci.* **2009**, *4*, 313–322.

[30] Late, D. J.; Ghosh, A.; Chakraborty, B.; Sood, A. K.; Waghmare, U. V; Rao, C. N. R. Molecular Charge-Transfer Interaction with Single-Layer Graphene. *J. Exp. Nanosci.* **2011**, *6*, 641–651.

[31] Late, D. J.; Ghosh, A.; Subrahmanyam, K. S.; Panchakarla, L. S.; Krupanidhi, S. B.; Rao, C. N. R. Characteristics of Field-Effect Transistors Based on Undoped and B- and N-Doped Few-Layer Graphenes. *Solid State Commun.* **2010**, *150*, 734–738.

[32] Late, D. J.; Maitra, U.; Panchakarla, L. S.; Waghmare, U. V; Rao, C. N. R. Temperature Effects on the Raman Spectra of Graphenes: Dependence on the Number of Layers and Doping. *J. Phys. Condens. Matter* **2011**, *23*, 055303.

[33] Maitra, U.; Gupta, U.; De, M.; Datta, R.; Govindaraj, A.; Rao, C. N. R. Highly Effective Visible-Light-Induced H2 Generation by Single-Layer 1T-MoS2 and a Nanocomposite of Few-Layer 2H-MoS2 with Heavily Nitrogenated Graphene. *Angew. Chemie Int. Ed.* **2013**, *52*, 13057–13061.

[34] Yan, C.; Kim, K.-S.; Lee, S.-K.; Bae, S.-H.; Hong, B. H.; Kim, J.-H.; Lee, H.-J.; Ahn, J.-H. Mechanical and Environmental Stability of Polymer Thin-Film-Coated Graphene. *ACS Nano* **2011**, *6*, 2096–2103.

[35] Yi, L.; Yin, Z.; Zhang, Y.; Chang, T. A Theoretical Evaluation of the Temperature and Strain-Rate Dependent Fracture Strength of Tilt Grain Boundaries in Graphene. *Carbon N. Y.* **2013**, *51*, 373–380.

[36] Rao, C. N. R.; Subrahmanyam, K. S.; Ramakrishna Matte, H. S. S.; Abdulhakeem, B.; Govindaraj, a; Das, B.; Kumar, P.; Ghosh, A.; Late, D. J. A Study of the Synthetic Methods and Properties of Graphenes. *Sci. Technol. Adv. Mater.* **2010**, *11*, 054502.

[37] Gopinadhan, K.; Shin, Y. J.; Yudhistira, I.; Niu, J.; Yang, H. Giant Magnetoresistance in Single-Layer Graphene Flakes with a Gate-Voltage-Tunable Weak Antilocalization. *Phys. Rev. B* **2013**, *88*, 195429.

[38] Bolotin, K. I.; Sikes, K. J.; Jiang, Z.; Klima, M.; Fudenberg, G.; Hone, J.; Kim, P.; Stormer, H. L. Ultrahigh Electron Mobility in Suspended Graphene. *Solid State Commun.* **2008**, *146*, 351–355.

[39] Hwang, E. H.; Das Sarma, S. Acoustic Phonon Scattering Limited Carrier Mobility in Two-Dimensional Extrinsic Graphene. *Phys. Rev. B* **2008**, *77*, 115449.

[40] Hong, X.; Posadas, A.; Zou, K.; Ahn, C. H.; Zhu, J. High-Mobility Few-Layer Graphene Field Effect Transistors Fabricated on Epitaxial Ferroelectric Gate Oxides. *Phys. Rev. Lett.* **2009**, *102*, 136808.

[41] Kim, K. S.; Zhao, Y.; Jang, H.; Lee, S. Y.; Kim, J. M.; Kim, K. S.; Ahn, J.-H.; Kim, P.; Choi, J.-Y.; Hong, B. H. Large-Scale Pattern Growth of Graphene Films for Stretchable Transparent Electrodes. *Nature* **2009**, *457*, 706–710.

[42] Martin, J.; Akerman, N.; Ulbricht, G.; Lohmann, T.; Smet, J. H.; von Klitzing, K.; Yacoby, a. Observation of Electron-Hole Puddles in Graphene Using a Scanning Single Electron Transistor. *Nat Phys* **2007**, *4*, 13.

[43] Stoller, M. D.; Park, S.; Yanwu, Z.; An, J.; Ruoff, R. S. Graphene-Based Ultracapacitors. *Nano Lett.* **2008**, *8*, 3498–3502.

[44] Nair, R. R.; Blake, P.; Grigorenko, A. N.; Novoselov, K. S.; Booth, T. J.; Stauber, T.; Peres, N. M. R.; Geim, A. K. Fine Structure Constant Defines Visual Transparency of Graphene. *Sci.* **2008**, *320* , 1308.

[45] Novoselov, K. S.; Geim, a K.; Morozov, S. V; Jiang, D.; Katsnelson, M. I.; Grigorieva, I. V; Dubonos, S. V; Firsov, a a. Two-Dimensional Gas of Massless Dirac Fermions in Graphene. *Nature* **2005**, *438*, 197–200.

[46] Latil, S.; Henrard, L. Charge Carriers in Few-Layer Graphene Films. *Phys. Rev. Lett.* **2006**, *97*, 1–4.

[47] Dao, V.-D.; Larina, L. L.; Jung, K.-D.; Lee, J.-K.; Choi, H.-S. Graphene-NiO Nanohybrid Prepared by Dry Plasma Reduction as a Low-Cost Counter Electrode Material for Dye-Sensitized Solar Cells. *Nanoscale* **2014**, *6*, 477–482.

[48] Gómez-Navarro, C.; Weitz, R. T.; Bittner, A. M.; Scolari, M.; Mews, A.; Burghard, M.; Kern, K. Electronic Transport Properties of Individual Chemically Reduced Graphene Oxide Sheets. *Nano Lett.* **2007**, *7*, 3499–3503.

[49] Zhang, F.; Hou, C.; Zhang, Q.; Wang, H.; Li, Y. Graphene Sheets/cobalt Nanocomposites as Low-Cost/high-Performance Catalysts for Hydrogen Generation. *Mater. Chem. Phys.* **2012**, *135*, 826–831.

[50] Zhang, S.; Shao, Y.; Liu, J.; Aksay, I. A.; Lin, Y. Graphene–Polypyrrole Nanocomposite as a Highly Efficient and Low Cost Electrically Switched Ion Exchanger for Removing $ClO_4^-$ from Wastewater. *ACS Appl. Mater. Interfaces* **2011**, *3*, 3633–3637.

[51] Frey, G. L.; Reynolds, K. J.; Friend, R. H. Novel Electrodes from Solution-Processed Layer-Structure Materials. *Adv. Mater.* **2002**, *14*, 265–268.

[52] Ellis, J. K.; Lucero, M. J.; Scuseria, G. E. The Indirect to Direct Band Gap Transition in Multilayered $MoS_2$ as Predicted by Screened Hybrid Density Functional Theory. *Appl. Phys. Lett.* **2011**, *99*, 261908.

[53] Cheiwchanchamnangij, T.; Lambrecht, W. R. L. Quasiparticle Band Structure Calculation of Monolayer, Bilayer, and Bulk $MoS_2$. *Phys. Rev. B - Condens. Matter Mater. Phys.* **2012**, *85*, 205302.

[54] Han, S. W.; Kwon, H.; Kim, S. K.; Ryu, S.; Yun, W. S.; Kim, D. H.; Hwang, J. H.; Kang, J. S.; Baik, J.; Shin, H. J.; et al. Band-Gap Transition Induced by Interlayer van Der Waals Interaction in $MoS_2$. *Phys. Rev. B - Condens. Matter Mater. Phys.* **2011**, *84*, 45409.

[55] Albe, K.; Klein, A. Density-Functional-Theory Calculations of Electronic Band Structure of Single-Crystal and Single-Layer $WS_2$. *Phys. Rev. B* **2002**, *66*, 73413.

[56] Klein, a.; Tiefenbacher, S.; Eyert, V.; Pettenkofer, C.; Jaegermann, W. Electronic Band Structure of Single-Crystal and Single-Layer $WS_2$: Influence of Interlayer van Der Waals Interactions. *Phys. Rev. B* **2001**, *64*, 205416.

[57] Wang, Q. H.; Kalantar-Zadeh, K.; Kis, A.; Coleman, J. N.; Strano, M. S. Electronics and Optoelectronics of Two-Dimensional Transition Metal Dichalcogenides. *Nat. Nanotechnol.* **2012**, *7*, 699–712.

[58] Kumar, A.; Ahluwalia, P. K. Electronic Structure of Transition Metal Dichalcogenides Monolayers 1H-$MX_2$ (M = Mo, W; X = S, Se, Te) from Ab-Initio Theory: New Direct Band Gap Semiconductors. *Eur. Phys. J. B* **2012**, *85*, 1–7.

[59] Terrones, H.; López-Urías, F.; Terrones, M. Novel Hetero-Layered Materials with Tunable Direct Band Gaps by Sandwiching Different Metal Disulfides and Diselenides. *Sci. Rep.* **2013**, *3*, 1549.

[60] Rycerz, A.; Tworzydlo, J.; Beenakker, C. W. J. Valley Filter and Valley Valve in Graphene. *Nat Phys* **2007**, *3*, 172–175.

[61] Garcia-Pomar, J. L.; Cortijo, A.; Nieto-Vesperinas, M. Fully Valley-Polarized Electron Beams in Graphene. *Phys. Rev. Lett.* **2008**, *100*, 236801.

[62] Lundeberg, M. B.; Folk, J. A. Harnessing Chirality for Valleytronics. *Sci.* **2014**, *346* , 422–423.

[63] Molina-Sánchez, A.; Wirtz, L. Phonons in Single-Layer and Few-Layer $MoS_2$ and $WS_2$. *Phys. Rev. B* **2011**, *84*, 155413.

[64] Kam, K. K.; Parkinson, B. A. Detailed Photocurrent Spectroscopy of the Semiconducting Group VIB Transition Metal Dichalcogenides. *J. Phys. Chem.* **1982**, *86*, 463–467.

[65] Lee, C.; Yan, H.; Brus, L. E.; Heinz, T. F.; Hone, J.; Ryu, S. Anomalous Lattice Vibrations of Single- and Few-Layer $MoS_2$. *ACS Nano* **2010**, *4*, 2695–2700.

[66] Mak, K. F.; He, K.; Shan, J.; Heinz, T. F. Control of Valley Polarization in Monolayer $MoS_2$ by Optical Helicity. *Nat Nano* **2012**, *7*, 494–498.

[67] Komsa, H. P.; Krasheninnikov, A. V. Effects of Confinement and Environment on the Electronic Structure and Exciton Binding Energy of $MoS_2$ from First Principles. *Phys. Rev. B - Condens. Matter Mater. Phys.* **2012**, *86*, 241201.

[68] Wan, R.; Jia, C.; Zhang, W. Preparation and Photoelectric Properties of P-$CaFe_2O_4$/n-$WO_3$ Composites. *J. Alloys Compd.* **2012**, *544*, 1–5.

[69] Zhong, H.; Yang, G.; Song, H.; Liao, Q.; Cui, H.; Shen, P.; Wang, C.-X. Vertically Aligned Graphene-Like $SnS_2$ Ultrathin Nanosheet Arrays: Excellent Energy Storage, Catalysis, Photoconduction, and Field-Emitting Performances. *J. Phys. Chem. C* **2012**, *116*, 9319–9326.

[70] Late, D. J.; Shaikh, P. A.; Khare, R.; Kashid, R. V; Chaudhary, M.; More, M. A.; Ogale, S. B. Pulsed Laser-Deposited $MoS_2$ Thin Films on W and Si: Field Emission and Photoresponse Studies. *ACS Appl. Mater. Interfaces* **2014**, *6*, 15881–15888.

[71] Mak, K. F.; Lee, C.; Hone, J.; Shan, J.; Heinz, T. F. Atomically Thin $MoS_2$: A New Direct-Gap Semiconductor. *Phys. Rev. Lett.* **2010**, *105*, 136805.

[72] Chang, C. H.; Fan, X.; Lin, S. H.; Kuo, J. L. Orbital Analysis of Electronic Structure and Phonon Dispersion in $MoS_2$, $MoSe_2$, $WS_2$, and $WSe_2$ Monolayers under Strain. *Phys. Rev. B - Condens. Matter Mater. Phys.* **2013**, *88*, 195420.

[73] Fuchtbauer, H. G.; Tuxen, A. K.; Moses, P. G.; Topsoe, H.; Besenbacher, F.; Lauritsen, J. V. Morphology and Atomic-Scale Structure of Single-Layer $WS_2$ Nanoclusters. *Phys. Chem. Chem. Phys.* **2013**, *15*, 15971–15980.

[74] Ghosh, C. K.; Sarkar, D.; Mitra, M. K.; Chattopadhyay, K. K. Equibiaxial Strain: Tunable Electronic Structure and Optical Properties of Bulk and Monolayer $MoSe_2$. *J. Phys. D. Appl. Phys.* **2013**, *46*, 395304.

[75] Late, D. J.; Shirodkar, S. N.; Waghmare, U. V; Dravid, V. P.; Rao, C. N. R. Thermal Expansion, Anharmonicity and Temperature-Dependent Raman Spectra of Single- and Few-Layer $MoSe_2$ and $WSe_2$. *ChemPhysChem* **2014**, *15*, 1592–1598.

[76] Late, D. J.; Liu, B.; Luo, J.; Yan, A.; Matte, H. S. S. R.; Grayson, M.; Rao, C. N. R.; Dravid, V. P. GaS and GaSe Ultrathin Layer Transistors. *Adv. Mater.* **2012**, *24*, 3549–3554.

[77] Late, D. J.; Liu, B.; Matte, H. S. S. R.; Rao, C. N. R.; Dravid, V. P. Rapid Characterization of Ultrathin Layers of Chalcogenides on $SiO_2$/Si Substrates. *Adv. Funct. Mater.* **2012**, *22*, 1894–1905.

[78] Moser, J.; Lévy, F. Random Stacking in $MoS_{2-x}$ Sputtered Thin Films. *Thin Solid Films* **1994**, *240*, 56–59.

[79] Schönfeld, B.; Huang, J. J.; Moss, S. C. Anisotropic Mean-Square Displacements (MSD) in Single-Crystals of 2 H - and 3 R -$MoS_2$. *Acta Crystallogr. Sect. B Struct. Sci.* **1983**, *39*, 404–407.

[80] Constantinescu, G.; Kuc, A.; Heine, T. Stacking in Bulk and Bilayer Hexagonal Boron Nitride. *Phys. Rev. Lett.* **2013**, *111*, 36104.

[81] He, J.; Hummer, K.; Franchini, C. Stacking Effects on the Electronic and Optical Properties of Bilayer Transition Metal Dichalcogenides $MoS_2$, $MoSe_2$. *Phys. Rev. B* **2014**, *89*, 075409.

[82] Beal, a R.; Knights, J. C.; Liang, W. Y. Transmission Spectra of Some Transition Metal Dichalcogenides. II. Group VIA: Trigonal Prismatic Coordination. *J. Phys. C Solid State Phys.* **2001**, *5*, 3540–3551.

(83) Kobayashi, K.; Yamauchi, J. Electronic Structure and Scanning-Tunneling-Microscopy Image of Molybdenum Dichalcogenide Surfaces. *Phys. Rev. B* **1995**, *51*, 17085–17095.

[84] Li, T.; Galli, G. Electronic Properties of $MoS_2$ Nanoparticles. *J. Phys. Chem. C* **2007**, *111*, 16192–16196.

[85] Liu, L.; Kumar, S. B.; Ouyang, Y.; Guo, J. Performance Limits of Monolayer Transition Metal Dichalcogenide Transistors. *IEEE Trans. Electron Devices* **2011**, *58*, 3042–3047.

[86] Ding, Y.; Wang, Y.; Ni, J.; Shi, L.; Shi, S.; Tang, W. First Principles Study of Structural, Vibrational and Electronic Properties of Graphene-like $MX_2$ (M=Mo, Nb, W, Ta; X=S, Se, Te) Monolayers. *Phys. B Condens. Matter* **2011**, *406*, 2254–2260.

[87] Ataca, C.; Şahin, H.; Ciraci, S. Stable, Single-Layer $MX_2$ Transition-Metal Oxides and Dichalcogenides in a Honeycomb-like Structure. *J. Phys. Chem. C* **2012**, *116*, 8983–8999.

[88] Lebègue, S.; Eriksson, O. Electronic Structure of Two-Dimensional Crystals from Ab-Initio Theory. *Phys. Rev. B* **2009**, *79*, 115409.

[89] Shen, C.-C.; Hsu, Y.-T.; Li, L.-J.; Liu, H.-L. Charge Dynamics and Electronic Structures of Monolayer $MoS_2$ Films Grown by Chemical Vapor Deposition. *Appl. Phys. Express* **2013**, *6*, 125801.

[90] Liu, D.; Guo, Y.; Fang, L.; Robertson, J. Sulfur Vacancies in Monolayer $MoS_2$ and Its Electrical Contacts. *Appl. Phys. Lett.* **2013**, *103*, 183113.

[91] Gutiérrez, H. R.; Perea-López, N.; Elías, A. L.; Berkdemir, A.; Wang, B.; Lv, R.; López-Urías, F.; Crespi, V. H.; Terrones, H.; Terrones, M. Extraordinary Room-Temperature Photoluminescence in Triangular $WS_2$ Monolayers. *Nano Lett.* **2012**, *13*, 3447–3454.

[92] Espejo, C.; Rangel, T.; Romero, a. H.; Gonze, X.; Rignanese, G. M. Band Structure Tunability in $MoS_2$ under Interlayer Compression: A DFT and GW Study. *Phys. Rev. B - Condens. Matter Mater. Phys.* **2013**, *87*, 245114.

[93] Berkdemir, A.; Gutiérrez, H. R.; Botello-Méndez, A. R.; Perea-López, N.; Elías, A. L.; Chia, C.-I.; Wang, B.; Crespi, V. H.; López-Urías, F.; Charlier, J.-C.; et al. Identification of Individual and Few Layers of $WS_2$ Using Raman Spectroscopy. *Sci. Rep.* **2013**, *3*, 1755.

[94] Zibouche, N.; Kuc, A.; Heine, T. From Layers to Nanotubes: Transition Metal Disulfides $TMS_2$. *Eur. Phys. J. B* **2012**, *85*.

[95] Jin, W.; Yeh, P. C.; Zaki, N.; Zhang, D.; Sadowski, J. T.; Al-Mahboob, A.; Van Der Zande, A. M.; Chenet, D. a.; Dadap, J. I.; Herman, I. P.; et al. Direct Measurement of the Thickness-Dependent Electronic Band Structure of $MoS_2$ Using Angle-Resolved Photoemission Spectroscopy. *Phys. Rev. Lett.* **2013**, *111*, 106801.

[96] Splendiani, A.; Sun, L.; Zhang, Y.; Li, T.; Kim, J.; Chim, C.-Y.; Galli, G.; Wang, F. Emerging Photoluminescence in Monolayer $MoS_2$. *Nano Lett.* **2010**, *10*, 1271–1275.

[97] Yin, Z.; Li, H.; Li, H.; Jiang, L.; Shi, Y.; Sun, Y.; Lu, G.; Zhang, Q.; Chen, X.; Zhang, H. Single-Layer $MoS_2$ Phototransistors. *ACS Nano* **2011**, *6*, 74–80.

[98] Mouri, S.; Miyauchi, Y.; Matsuda, K. Tunable Photoluminescence of Monolayer $MoS_2$ via Chemical Doping. *Nano Lett.* **2013**, *13*, 5944–5948.

[99] Nan, H.; Wang, Z.; Wang, W.; Liang, Z.; Lu, Y.; Chen, Q.; He, D.; Tan, P.; Miao, F.; Wang, X.; et al. Strong Photoluminescence Enhancement of $MoS_2$ through Defect Engineering and Oxygen Bonding. *ACS Nano* **2014**, *8*, 5738–5745.

[100] Tongay, S.; Zhou, J.; Ataca, C.; Lo, K.; Matthews, T. S.; Li, J.; Grossman, J. C.; Wu, J. Thermally Driven Crossover from Indirect toward Direct Bandgap in 2D Semiconductors: $MoSe_2$ versus $MoS_2$. *Nano Lett.* **2012**, *12*, 5576–5580.

[101] Zhao, W.; Ghorannevis, Z.; Chu, L.; Toh, M.; Kloc, C.; Tan, P. H.; Eda, G. Evolution of Electronic Structure in Atomically Thin Sheets of $WS_2$ and $WSe_2$. *ACS Nano* **2013**, *7*, 791–797.

[102] Liu, K.-K.; Zhang, W.; Lee, Y.-H.; Lin, Y.-C.; Chang, M.-T.; Su, C.-Y.; Chang, C.-S.; Li, H.; Shi, Y.; Zhang, H.; et al. Growth of Large-Area and Highly Crystalline $MoS_2$ Thin Layers on Insulating Substrates. *Nano Lett.* **2012**, *12*, 1538–1544.

[103] Balendhran, S.; Ou, J. Z.; Bhaskaran, M.; Sriram, S.; Ippolito, S.; Vasic, Z.; Kats, E.; Bhargava, S.; Zhuiykov, S.; Kalantar-zadeh, K. Atomically Thin Layers of $MoS_2$ via a Two Step Thermal Evaporation-Exfoliation Method. *Nanoscale* **2012**, *4*, 461–466.

[104] Shi, Y.; Zhou, W.; Lu, A.-Y.; Fang, W.; Lee, Y.-H.; Hsu, A. L.; Kim, S. M.; Kim, K. K.; Yang, H. Y.; Li, L.-J.; et al. Van Der Waals Epitaxy of $MoS_2$ Layers Using Graphene As Growth Templates. *Nano Lett.* **2012**, *12*, 2784–2791.

[105] Peng, Y.; Meng, Z.; Zhong, C.; Lu, J.; Yu, W.; Yang, Z.; Qian, Y. Hydrothermal Synthesis of $MoS_2$ and Its Pressure-Related Crystallization. *J. Solid State Chem.* **2001**, *159*, 170–173.

[106] Peng, Y.; Meng, Z.; Zhong, C.; Lu, J.; Yu, W.; Jia, Y.; Qian, Y. Hydrothermal Synthesis and Characterization of Single-Molecular-Layer $MoS_2$ and $MoSe_2$. *Chem. Lett.* **2001**, *30*, 772–773.

[107] Frindt, R. F. The Optical Properties of Single Crystals of $WSe_2$ and $MoTe_2$. *J. Phys. Chem. Solids* **1963**, *24*, 1107–1108.

[108] Frindt, R. F.; Yoffe, A. D. Physical Properties of Layer Structures: Optical Properties and Photoconductivity of Thin Crystals of Molybdenum Disulphide. *Proc. R. Soc. London A Math. Phys. Eng. Sci.* **1963**, *273*, 69–83.

[109] Ramasubramaniam, A. Large Excitonic Effects in Monolayers of Molybdenum and Tungsten Dichalcogenides. *Phys. Rev. B - Condens. Matter Mater. Phys.* **2012**, *86*, 115409.

[110] Song, Y.; Dery, H. Transport Theory of Monolayer Transition-Metal Dichalcogenides through Symmetry. *Phys. Rev. Lett.* **2013**, *111*, 26601.

[111] Salvatore, G. A.; Münzenrieder, N.; Barraud, C.; Petti, L.; Zysset, C.; Büthe, L.; Ensslin, K.; Tröster, G. Fabrication and Transfer of Flexible Few-Layers $MoS_2$ Thin Film Transistors to Any Arbitrary Substrate. *ACS Nano* **2013**, *7*, 8809–8815.

[112] Castellanos-Gomez, A.; Poot, M.; Steele, G. A.; van der Zant, H. S. J.; Agraït, N.; Rubio-Bollinger, G. Elastic Properties of Freely Suspended $MoS_2$ Nanosheets. *Adv. Mater.* **2012**, *24*, 772–775.

[113] Huang, X.; Zeng, Z.; Zhang, H. Metal Dichalcogenide Nanosheets: Preparation, Properties and Applications. *Chem. Soc. Rev.* **2013**, *42*, 1934–1946.

[114] Bertolazzi, S.; Brivio, J.; Kis, A. Stretching and Breaking of Ultrathin $MoS_2$. *ACS Nano* **2011**, *5*, 9703–9709.

[115] Castellanos-Gomez, A.; Poot, M.; Steele, G.; van der Zant, H.; Agraït, N.; Rubio-Bollinger, G. Mechanical Properties of Freely Suspended Semiconducting Graphene-like Layers Based on $MoS_2$. *Nanoscale Res. Lett.* **2012**, *7*, 1–4.

[116] Sahin, H.; Tongay, S.; Horzum, S.; Fan, W.; Zhou, J.; Li, J.; Wu, J.; Peeters, F. M. Anomalous Raman Spectra and Thickness-Dependent Electronic Properties of $WSe_2$. *Phys. Rev. B - Condens. Matter Mater. Phys.* **2013**, *87*, 165409.

[117] Luo, X.; Zhao, Y.; Zhang, J.; Toh, M.; Kloc, C.; Xiong, Q.; Quek, S. Y. Effects of Lower Symmetry and Dimensionality on Raman Spectra in Two-Dimensional $WSe_2$. *Phys. Rev. B - Condens. Matter Mater. Phys.* **2013**, *88*, 195313.

[118] Thripuranthaka, M.; Kashid, R. V; Sekhar Rout, C.; Late, D. J. Temperature Dependent Raman Spectroscopy of Chemically Derived Few Layer $MoS_2$ and $WS_2$ Nanosheets. *Appl. Phys. Lett.* **2014**, *104*, 081911.

[119] Castellanos-Gomez, A.; Roldán, R.; Cappelluti, E.; Buscema, M.; Guinea, F.; van der Zant, H. S. J.; Steele, G. A. Local Strain Engineering in Atomically Thin $MoS_2$. *Nano Lett.* **2013**, *13*, 5361–5366.

[120] Johari, P.; Shenoy, V. B. Tuning the Electronic Properties of Semiconducting Transition Metal Dichalcogenides by Applying Mechanical Strains. *ACS Nano* **2012**, *6*, 5449–5456.

[121] He, K.; Poole, C.; Mak, K. F.; Shan, J. Experimental Demonstration of Continuous Electronic Structure Tuning via Strain in Atomically Thin $MoS_2$. *Nano Lett.* **2013**, *13*, 2931–2936.

[122] Scalise, E.; Houssa, M.; Pourtois, G.; Afanas'ev, V.; Stesmans, A. Strain-Induced Semiconductor to Metal Transition in the Two-Dimensional Honeycomb Structure of $MoS_2$. *Nano Res.* **2012**, *5*, 43–48.

[123] Li, H.; Zhang, Q.; Yap, C. C. R.; Tay, B. K.; Edwin, T. H. T.; Olivier, A.; Baillargeat, D. From Bulk to Monolayer $MoS_2$: Evolution of Raman Scattering. *Adv. Funct. Mater.* **2012**, *22*, 1385–1390.

[124] Lanzillo, N. A.; Glen Birdwell, A.; Amani, M.; Crowne, F. J.; Shah, P. B.; Najmaei, S.; Liu, Z.; Ajayan, P. M.; Lou, J.; Dubey, M.; et al. Temperature-Dependent Phonon Shifts in Monolayer $MoS_2$. *Appl. Phys. Lett.* **2013**, *103*, 093102.

[125] Najmaei, S.; Liu, Z.; Ajayan, P. M.; Lou, J. Thermal Effects on the Characteristic Raman Spectrum of Molybdenum Disulfide ($MoS_2$) of Varying Thicknesses. *Appl. Phys. Lett.* **2012**, *100*, 013106.

[126] Thripuranthaka, M.; Late, D. J. Temperature Dependent Phonon Shifts in Single-Layer $WS_2$. *ACS Appl. Mater. Interfaces* **2014**, *6*, 1158–1163.

[127] Chakraborty, B.; Bera, A.; Muthu, D. V. S.; Bhowmick, S.; Waghmare, U. V.; Sood, a. K. Symmetry-Dependent Phonon Renormalization in Monolayer $MoS_2$ Transistor. *Phys. Rev. B - Condens. Matter Mater. Phys.* **2012**, *85*, 161403.

[128] Conley, H. J.; Wang, B.; Ziegler, J. I.; Haglund, R. F.; Pantelides, S. T.; Bolotin, K. I. Bandgap Engineering of Strained Monolayer and Bilayer $MoS_2$. *Nano Lett.* **2013**, *13*, 3626–3630.

[129] Das, S.; Chen, H.-Y.; Penumatcha, A. V.; Appenzeller, J. High Performance Multilayer $MoS_2$ Transistors with Scandium Contacts. *Nano Lett.* **2012**, *13*, 100–105.

[130] Dashora, A.; Ahuja, U.; Venugopalan, K. Electronic and Optical Properties of $MoS_2$ (0 0 0 1) Thin Films: Feasibility for Solar Cells. *Comput. Mater. Sci.* **2013**, *69*, 216–221.

[131] Radisavljevic, B.; Radenovic, a; Brivio, J.; Giacometti, V.; Kis, a; RadisavljevicB.; RadenovicA.; BrivioJ.; GiacomettiV.; KisA. Single-Layer $MoS_2$ Transistors. *Nat Nano* **2011**, *6*, 147–150.

[132] Sahoo, S.; Gaur, A. P. S.; Ahmadi, M.; Guinel, M. J.-F.; Katiyar, R. S. Temperature-Dependent Raman Studies and Thermal Conductivity of Few-Layer $MoS_2$. *J. Phys. Chem. C* **2013**, *117*, 9042–9047.

[133] Zhang, Y.; Zhang, Y.; Ji, Q.; Ju, J.; Yuan, H.; Shi, J.; Gao, T.; Ma, D.; Liu, M.; Chen, Y.; et al. Controlled Growth of High-Quality Monolayer $WS_2$ Layers on Sapphire and Imaging Its Grain Boundary. *ACS Nano* **2013**, *7*, 8963–8971.

[134] Perea-López, N.; Elías, A. L.; Berkdemir, A.; Castro-Beltran, A.; Gutiérrez, H. R.; Feng, S.; Lv, R.; Hayashi, T.; López-Urías, F.; Ghosh, S.; et al. Photosensor Device Based on Few-Layered $WS_2$ Films. *Adv. Funct. Mater.* **2013**, *23*, 5511–5517.

[135] Ma, Y.; Dai, Y.; Guo, M.; Niu, C.; Lu, J.; Huang, B. Electronic and magnetic properties of perfect, vacancy-doped, and nonmetal adsorbed $MoSe_2$, $MoTe_2$ and $WS_2$ monolayers. *Phys. Chem. Chem. Phys.* **2011**, *13*, 15546–15553.

[136] Jäger-Waldau, A.; Lux-Steiner, M.; Jäger-Waldau, R.; Burkhardt, R.; Bucher, E. Composition and Morphology of $MoSe_2$ Thin Films. *Thin Solid Films* **1990**, *189*, 339–345.

[137] Tonndorf, P.; Schmidt, R.; Böttger, P.; Zhang, X.; Börner, J.; Liebig, A.; Albrecht, M.; Kloc, C.; Gordan, O.; Zahn, D. R. T.; et al. Photoluminescence Emission and Raman Response of Monolayer $MoS_2$, $MoSe_2$, and $WSe_2$. *Opt. Express* **2013**, *21*, 4908–4916.

[138] Fang, H.; Chuang, S.; Chang, T. C.; Takei, K.; Takahashi, T.; Javey, A. High-Performance Single Layered $WSe_2$ p-FETs with Chemically Doped Contacts. *Nano Lett.* **2012**, *12*, 3788–3792.

[139] Conan, A.; Bonnet, A.; Amrouche, A.; Spiesser, M. Semiconducting Properties and Band Structure of $MoTe_2$ Single Crystals. *J. Phys. Fr.* **1984**, *45*, 459–465.

[140] Mar, A.; Jobic, S.; Ibers, J. a. Metal-Metal vs Tellurium-Tellurium Bonding in $WTe_2$ and Its Ternary Variants $TaIrTe_4$ and $NbIrTe_4$. *J. Am. Chem. Soc.* **1992**, *114*, 8963–8971.

[141] Kabashima, S. Electrical Properties of Tungsten-Ditelluride $WTe_2$. *J. Phys. Soc. Japan* **1966**, *21*, 945–948.

[142] Liu, F.; Shimotani, H.; Shang, H.; Kanagasekaran, T.; Zólyomi, V.; Drummond, N.; Fal'ko, V. I.; Tanigaki, K. High-Sensitivity Photodetectors Based on Multilayer GaTe Flakes. *ACS Nano* **2013**, *8*, 752–760.

[143] Amato, G.; Manfredotti, C.; Meliga, M.; Mellano, W. InSe Photoelectrochemical Solar Cells. *Sol. Cells* **1984**, *13*, 19–28.

[144] Feng, W.; Zheng, W.; Cao, W.; Hu, P. Back Gated Multilayer InSe Transistors with Enhanced Carrier Mobilities via the Suppression of Carrier Scattering from a Dielectric Interface. *Adv. Mater.* **2014**, *26*, 6587–6593.

[145] Sánchez-Royo, J.; Muñoz-Matutano, G.; Brotons-Gisbert, M.; Martínez-Pastor, J.; Segura, A.; Cantarero, A.; Mata, R.; Canet-Ferrer, J.; Tobias, G.; Canadell, E.; et al. Electronic Structure, Optical Properties, and Lattice Dynamics in Atomically Thin Indium Selenide Flakes. *Nano Res.* **2014**, *7*, 1556–1568.

[146] Segura, A.; Guesdon, J. P.; Besson, J. M.; Chevy, A. Photoconductivity and Photovoltaic Effect in Indium Selenide. *J. Appl. Phys.* **1983**, *54*.

[147] Tamalampudi, S. R.; Lu, Y.-Y.; Kumar U., R.; Sankar, R.; Liao, C.-D.; Moorthy B., K.; Cheng, C.-H.; Chou, F. C.; Chen, Y.-T. High Performance and Bendable Few-Layered InSe Photodetectors with Broad Spectral Response. *Nano Lett.* **2014**, *14*, 2800–2806.

[148] Li, L.; Yu, Y.; Ye, G. J.; Ge, Q.; Ou, X.; Wu, H.; Feng, D.; Chen, X. H.; Zhang, Y. Black Phosphorus Field-Effect Transistors. *Nat Nano* **2014**, *9*, 372–377.

[149] Mas-Ballesté, R.; Gómez-Navarro, C.; Gómez-Herrero, J.; Zamora, F. 2D Materials: To Graphene and Beyond. *Nanoscale* **2011**, *3*, 20–30.

[150] Maitra, U.; Matte, H. S. S. R.; Kumar, P.; Rao, C. N. R. Strategies for the Synthesis of Graphene, Graphene Nanoribbons, Nanoscrolls and Related Materials. *CHIMIA International Journal for Chemistry*, *66*, 941–948.

[151] Sangwan, V. K.; Arnold, H. N.; Jariwala, D.; Marks, T. J.; Lauhon, L. J.; Hersam, M. C. Low-Frequency Electronic Noise in Single-Layer $MoS_2$ Transistors. *Nano Lett.* **2013**, *13*, 4351–4355.

[152] Chen, J.-R.; Odenthal, P. M.; Swartz, A. G.; Floyd, G. C.; Wen, H.; Luo, K. Y.; Kawakami, R. K. Control of Schottky Barriers in Single Layer $MoS_2$ Transistors with Ferromagnetic Contacts. *Nano Lett.* **2013**, *13*, 3106–3110.

[153] Jariwala, D.; Sangwan, V. K.; Late, D. J.; Johns, J. E.; Dravid, V. P.; Marks, T. J.; Lauhon, L. J.; Hersam, M. C. Band-like Transport in High Mobility Unencapsulated Single-Layer $MoS_2$ Transistors. *Appl. Phys. Lett.* **2013**, *102*, 173107.

[154] Late, D. J.; Liu, B.; Matte, H. S. S. R.; Dravid, V. P.; Rao, C. N. R. Hysteresis in Single-Layer $MoS_2$ Field Effect Transistors. *ACS Nano* **2012**, *6*, 5635–5641.

[155] O'Neill, A.; Khan, U.; Coleman, J. N. Preparation of High Concentration Dispersions of Exfoliated $MoS_2$ with Increased Flake Size. *Chem. Mater.* **2012**, *24*, 2414–2421.

[156] Frindt, R. F.; Arrott, A. S.; Curzon, A. E.; Heinrich, B.; Morrison, S. R.; Templeton, T. L.; Divigalpitiya, R.; Gee, M. A.; Joensen, P.; Schurer, P. J.; et al. Exfoliated $MoS_2$ Monolayers as Substrates for Magnetic Materials. *J. Appl. Phys.* **1991**, *70*.

[157] Ramakrishna Matte, H. S. S.; Gomathi, a.; Manna, A. K.; Late, D. J.; Datta, R.; Pati, S. K.; Rao, C. N. R. $MoS_2$ and $WS_2$ Analogues of Graphene. *Angew. Chemie - Int. Ed.* **2010**, *49*, 4059–4062.

[158] Gong, C.; Huang, C.; Miller, J.; Cheng, L.; Hao, Y.; Cobden, D.; Kim, J.; Ruoff, R. S.; Wallace, R. M.; Cho, K.; et al. Metal Contacts on Physical Vapor Deposited Monolayer $MoS_2$. *ACS Nano* **2013**, *7*, 11350–11357.

[159] Chen; Fan, R. Low-Temperature Hydrothermal Synthesis of Transition Metal Dichalcogenides. *Chem. Mater.* **2001**, *13*, 802–805.

[160] Matte, H. S. S. R.; Maitra, U.; Kumar, P.; Govinda Rao, B.; Pramoda, K.; Rao, C. N. R. Synthesis, Characterization, and Properties of Few-Layer Metal Dichalcogenides and Their Nanocomposites with Noble Metal Particles, Polyaniline, and Reduced Graphene Oxide. *Zeitschrift fur Anorg. und Allg. Chemie* **2012**, *638*, 2617–2624.

[161] Lee, Y.-H.; Zhang, X.-Q.; Zhang, W.; Chang, M.-T.; Lin, C.-T.; Chang, K.-D.; Yu, Y.-C.; Wang, J. T.-W.; Chang, C.-S.; Li, L.-J.; et al. Synthesis of Large-Area $MoS_2$ Atomic Layers with Chemical Vapor Deposition. *Adv. Mater.* **2012**, *24*, 2320–2325.

[162] Coleman, J. N.; Lotya, M.; O'Neill, A.; Bergin, S. D.; King, P. J.; Khan, U.; Young, K.; Gaucher, A.; De, S.; Smith, R. J.; et al. Two-Dimensional Nanosheets Produced by Liquid Exfoliation of Layered Materials. *Sci.* **2011**, *331* , 568–571.

[163] Eda, G.; Yamaguchi, H.; Voiry, D.; Fujita, T.; Chen, M.; Chhowalla, M. Photoluminescence from Chemically Exfoliated $MoS_2$. *Nano Lett.* **2011**, *11*, 5111–5116.

[164] Kim, S.; Konar, A.; Hwang, W.-S.; Lee, J. H.; Lee, J.; Yang, J.; Jung, C.; Kim, H.; Yoo, J.-B.; Choi, J.-Y.; et al. High-Mobility and Low-Power Thin-Film Transistors Based on Multilayer $MoS_2$ Crystals. *Nat Commun* **2012**, *3*, 1011.

[165] Bao, W.; Cai, X.; Kim, D.; Sridhara, K.; Fuhrer, M. S. High Mobility Ambipolar $MoS_2$ Field-Effect Transistors: Substrate and Dielectric Effects. *Appl. Phys. Lett.* **2013**, *102*, 042104.

[166] Li, X.; Magnuson, C. W.; Venugopal, A.; An, J.; Suk, J. W.; Han, B.; Borysiak, M.; Cai, W.; Velamakanni, A.; Zhu, Y.; et al. Graphene Films with Large Domain Size by a Two-Step Chemical Vapor Deposition Process. *Nano Lett.* **2010**, *10*, 4328–4334.

[167] Li, X.-L.; Ge, J.-P.; Li, Y.-D. Atmospheric Pressure Chemical Vapor Deposition: An Alternative Route to Large-Scale $MoS_2$ and $WS_2$ Inorganic Fullerene-like Nanostructures and Nanoflowers. *Chem. – A Eur. J.* **2004**, *10*, 6163–6171.

[168] Zhan, Y.; Liu, Z.; Najmaei, S.; Ajayan, P. M.; Lou, J. Large-Area Vapor-Phase Growth and Characterization of $MoS_2$ Atomic Layers on a $SiO_2$ Substrate. *Small* **2012**, *8*, 966–971.

[169] Perkins, F. K.; Friedman, A. L.; Cobas, E.; Campbell, P. M.; Jernigan, G. G.; Jonker, B. T. Chemical Vapor Sensing with Monolayer $MoS_2$. *Nano Lett.* **2013**, *13*, 668–673.

[170] Wang, X.; Feng, H.; Wu, Y.; Jiao, L. Controlled Synthesis of Highly Crystalline $MoS_2$ Flakes by Chemical Vapor Deposition. *J. Am. Chem. Soc.* **2013**, *135*, 5304–5307.

[171] Lin, Y.-C.; Zhang, W.; Huang, J.-K.; Liu, K.-K.; Lee, Y.-H.; Liang, C.-T.; Chu, C.-W.; Li, L.-J. Wafer-Scale $MoS_2$ Thin Layers Prepared by $MoO_3$ Sulfurization. *Nanoscale* **2012**, *4*, 6637–6641.

[172] Liu, Y.; Qiao, Y.; Zhang, W.-X.; Li, Z.; Hu, X.-L.; Yuan, L.-X.; Huang, Y.-H. Coral-like A-MnS Composites with N-Doped Carbon as Anode Materials for High-Performance Lithium-Ion Batteries. *J. Mater. Chem.* **2012**, *22*, 24026.

[173] Wang, M.; Li, G.; Xu, H.; Qian, Y.; Yang, J. Enhanced Lithium Storage Performances of Hierarchical Hollow $MoS_2$ Nanoparticles Assembled from Nanosheets. *ACS Appl. Mater. Interfaces* **2013**, *5*, 1003–1008.

[174] Harpeness, R.; Gedanken, A.; Weiss, a. M.; Slifkin, M. a. Microwave-Assisted Synthesis of Nanosized $MoSe_2$. *J. Mater. Chem.* **2003**, *13*, 2603–2606.

[175] Kundu, P.; Nethravathi, C.; Deshpande, P. A.; Rajamathi, M.; Madras, G.; Ravishankar, N. Ultrafast Microwave-Assisted Route to Surfactant-Free Ultrafine Pt Nanoparticles on Graphene: Synergistic Co-Reduction Mechanism and High Catalytic Activity. *Chem. Mater.* **2011**, *23*, 2772–2780.

[176] Zhu, Y.; Murali, S.; Stoller, M. D.; Velamakanni, A.; Piner, R. D.; Ruoff, R. S. Microwave Assisted Exfoliation and Reduction of Graphite Oxide for Ultracapacitors. *Carbon N. Y.* **2010**, *48*, 2118–2122.

[177] Edwards, R. S.; Coleman, K. S. Graphene Synthesis: Relationship to Applications. *Nanoscale* **2013**, *5*, 38–51.

[178] Sreeprasad, T. S.; Nguyen, P.; Kim, N.; Berry, V. Controlled, Defect-Guided, Metal-Nanoparticle Incorporation onto $MoS_2$ via Chemical and Microwave Routes: Electrical, Thermal, and Structural Properties. *Nano Lett.* **2013**, *13*, 4434–4441.

[179] Chu, C.-Y.; Tsai, J.-T.; Sun, C.-L. Synthesis of PEDOT-Modified Graphene Composite Materials as Flexible Electrodes for Energy Storage and Conversion Applications. *Int. J. Hydrogen Energy* **2012**, *37*, 13880–13886.

[180] Liu, J.; Xue, Y.; Zhang, M.; Dai, L. Graphene-Based Materials for Energy Applications. *MRS Bull.* **2012**, *37*, 1265–1272.

[181] Jiang, H.; Ma, J.; Li, C. Hierarchical Porous $NiCo_2O_4$ Nanowires for High-Rate Supercapacitors. *Chem. Commun.* **2012**, *48*, 4465–4467.

[182] Huang, Y.; Liang, J.; Chen, Y. An Overview of the Applications of Graphene-Based Materials in Supercapacitors. *Small* **2012**, *8*, 1805–1834.

[183] Wang, Q.; Wen, Z. H.; Li, J. H. A Hybrid Supercapacitor Fabricated with a Carbon Nanotube Cathode and a $TiO_2$–B Nanowire Anode. *Adv. Funct. Mater.* **2006**, *16*, 2141–2146.

[184] Cao, L.; Yang, S.; Gao, W.; Liu, Z.; Gong, Y.; Ma, L.; Shi, G.; Lei, S.; Zhang, Y.; Zhang, S.; et al. Direct Laser-Patterned Micro-Supercapacitors from Paintable $MoS_2$ Films. *Small* **2013**, *9*, 2905–2910.

[185] Shi, Y.; Wang, Y.; Wong, J. I.; Tan, A. Y. S.; Hsu, C.-L.; Li, L.-J.; Lu, Y.-C.; Yang, H. Y. Self-Assembly of Hierarchical $MoS_x$/CNT Nanocomposites ($2<x<3$): Towards High Performance Anode Materials for Lithium Ion Batteries. *Sci. Rep.* **2013**, *3*.

[186] Ramadoss, A.; Kim, T.; Kim, G.-S.; Kim, S. J. Enhanced Activity of a Hydrothermally Synthesized Mesoporous $MoS_2$ Nanostructure for High Performance Supercapacitor Applications. *New J. Chem.* **2014**, *38*, 2379–2385.

[187] Feng, J.; Sun, X.; Wu, C.; Peng, L.; Lin, C.; Hu, S.; Yang, J.; Xie, Y. Metallic Few-Layered $VS_2$ Ultrathin Nanosheets: High Two-Dimensional Conductivity for In-Plane Supercapacitors. *J. Am. Chem. Soc.* **2011**, *133*, 17832–17838.

[188] Devillers, N.; Jemei, S.; Péra, M.-C.; Bienaimé, D.; Gustin, F. Review of Characterization Methods for Supercapacitor Modelling. *J. Power Sources* **2014**, *246*, 596–608.

[189] Feng, H.; Wang, B.; Tan, L.; Chen, N.; Wang, N.; Chen, B. Polypyrrole/hexadecylpyridinium Chloride-Modified Graphite Oxide Composites: Fabrication, Characterization, and Application in Supercapacitors. *J. Power Sources* **2014**, *246*, 621–628.

[190] Guo, C.; Li, N.; Ji, L.; Li, Y.; Yang, X.; Lu, Y.; Tu, Y. N- and O-Doped Carbonaceous Nanotubes from Polypyrrole for Potential Application in High-Performance Capacitance. *J. Power Sources* **2014**, *247*, 660–666.

[191] Hsia, B.; Marschewski, J.; Wang, S.; In, J. Bin; Carraro, C.; Poulikakos, D.; Grigoropoulos, C. P.; Maboudian, R. Highly Flexible, All Solid-State Micro-Supercapacitors from Vertically Aligned Carbon Nanotubes. *Nanotechnology* **2014**, *25*, 055401.

[192] Kumar, A.; Singh, R. K.; Singh, H. K.; Srivastava, P.; Singh, R. Enhanced Capacitance and Stability of P-Toluenesulfonate Doped Polypyrrole/carbon Composite for Electrode Application in Electrochemical Capacitors. *J. Power Sources* **2014**, *246*, 800–807.

[193] Wang, B.; Park, J.; Su, D.; Wang, C.; Ahn, H.; Wang, G. Solvothermal Synthesis of $CoS_2$-Graphene Nanocomposite Material for High-Performance Supercapacitors. *J. Mater. Chem.* **2012**, *22*, 15750–15756.

[194] Yang, Z.; Xu, F.; Zhang, W.; Mei, Z.; Pei, B.; Zhu, X. Controllable Preparation of Multishelled NiO Hollow Nanospheres via Layer-by-Layer Self-Assembly for Supercapacitor Application. *J. Power Sources* **2014**, *246*, 24–31.

[195] Yeo, J.; Kim, G.; Hong, S.; Kim, M. S.; Kim, D.; Lee, J.; Lee, H. B.; Kwon, J.; Suh, Y. D.; Kang, H. W.; et al. Flexible Supercapacitor Fabrication by Room Temperature Rapid Laser Processing of Roll-to-Roll

Printed Metal Nanoparticle Ink for Wearable Electronics Application. *J. Power Sources* **2014**, *246*, 562–568.

[196] Zhang, J.; Tian, T.; Chen, Y.; Niu, Y.; Tang, J.; Qin, L.-C. Synthesis of Graphene from Dry Ice in Flames and Its Application in Supercapacitors. *Chem. Phys. Lett.* **2014**, *591*, 78–81.

[197] Zhang, X.; Zeng, X.; Yang, M.; Qi, Y. Investigation of a Branchlike $MoO_3$/Polypyrrole Hybrid with Enhanced Electrochemical Performance Used as an Electrode in Supercapacitors. *ACS Appl. Mater. Interfaces* **2013**, *6*, 1125–1130.

[198] Huang, K.-J.; Wang, L.; Liu, Y.-J.; Liu, Y.-M.; Wang, H.-B.; Gan, T.; Wang, L.-L. Layered $MoS_2$–graphene Composites for Supercapacitor Applications with Enhanced Capacitive Performance. *Int. J. Hydrogen Energy* **2013**, *38*, 14027–14034.

[199] Ratha, S.; Rout, C. S. Supercapacitor Electrodes Based on Layered Tungsten Disulfide-Reduced Graphene Oxide Hybrids Synthesized by a Facile Hydrothermal Method. *ACS Appl. Mater. Interfaces* **2013**, *5*, 11427–11433.

[200] Yu, G.; Hu, L.; Vosgueritchian, M.; Wang, H.; Xie, X.; McDonough, J. R.; Cui, X.; Cui, Y.; Bao, Z. Solution-Processed graphene/$MnO_2$ Nanostructured Textiles for High-Performance Electrochemical Capacitors. *Nano Lett.* **2011**, *11*, 2905–2911.

[201] Bernardi, M.; Palummo, M.; Grossman, J. C. Extraordinary Sunlight Absorption and One Nanometer Thick Photovoltaics Using Two-Dimensional Monolayer Materials. *Nano Lett.* **2013**, *13*, 3664–3670.

[202] Chang, H.; Wu, H. Graphene-Based Nanocomposites: Preparation, Functionalization, and Energy and Environmental Applications. *Energy Environ. Sci.* **2013**, *6*, 3483.

[203] Dodoo-Arhin, D.; Fabiane, M.; Bello, A.; Manyala, N. Graphene: Synthesis, Transfer, and Characterization for Dye-Sensitized Solar Cells Applications. *Ind. Eng. Chem. Res.* **2013**, *52*, 14160–14168.

[204] Hsiao, Y.; Lu, C.; Fang, T. To Enhance Performance of Light Soaking Process on ZnS / CuIn 1 − X Ga X Se 2 Solar Cell. **2013**, *2013*, 2–7.

[205] Lin, J.-Y.; Chan, C.-Y.; Chou, S.-W. Electrophoretic Deposition of Transparent $MoS_2$-Graphene Nanosheet Composite Films as Counter Electrodes in Dye-Sensitized Solar Cells. *Chem. Commun.* **2013**, *49*, 1440–1442.

[206] Shanmugam, M.; Durcan, C. a.; Yu, B. Layered Semiconductor Molybdenum Disulfide Nanomembrane Based Schottky-Barrier Solar Cells. *Nanoscale* **2012**, *4*, 7399–7405.

[207] Yue, G.; Lin, J.-Y.; Tai, S.-Y.; Xiao, Y.; Wu, J. A Catalytic Composite Film of $MoS_2$/graphene Flake as a Counter Electrode for Pt-Free Dye-Sensitized Solar Cells. *Electrochim. Acta* **2012**, *85*, 162–168.

[208] Zhou, L.-J.; Zhang, Y.-F.; Wu, L.-M. $SiC_2$ Siligraphene and Nanotubes: Novel Donor Materials in Excitonic Solar Cells. *Nano Lett.* **2013**, *13*, 5431–5436.

[209] Hsu, C.-M.; Battaglia, C.; Pahud, C.; Ruan, Z.; Haug, F.-J.; Fan, S.; Ballif, C.; Cui, Y. High-Efficiency Amorphous Silicon Solar Cell on a Periodic Nanocone Back Reflector. *Adv. Energy Mater.* **2012**, *2*, 628–633.

[210] Li, H.; Jia, R.; Chen, C.; Xing, Z.; Ding, W.; Meng, Y.; Wu, D.; Liu, X.; Ye, T. Influence of Nanowires Length on Performance of Crystalline Silicon Solar Cell. *Appl. Phys. Lett.* **2011**, *98*, 151116.

[211] Oh, J.; Yuan, H.-C.; Branz, H. M. An 18.2%-Efficient Black-Silicon Solar Cell Achieved through Control of Carrier Recombination in Nanostructures. *Nat. Nanotechnol.* **2012**, *7*, 743–748.

[212] Dewan, R.; Vasilev, I.; Jovanov, V.; Knipp, D. Optical Enhancement and Losses of Pyramid Textured Thin-Film Silicon Solar Cells. *J. Appl. Phys.* **2011**, *110*, 013101.

[213] Peters, M.; Rüdiger, M.; Hauser, H.; Hermle, M.; Bläsi, B. Diffractive Gratings for Crystalline Silicon Solar Cells—optimum Parameters and Loss Mechanisms. *Prog. Photovoltaics Res. Appl.* **2012**, *20*, 862–873.

[214] Yun, J.-M.; Noh, Y.-J.; Yeo, J.-S.; Go, Y.-J.; Na, S.-I.; Jeong, H.-G.; Kim, J.; Lee, S.; Kim, S.-S.; Koo, H. Y.; et al. Efficient Work-Function Engineering of Solution-Processed $MoS_2$ Thin-Films for Novel Hole and Electron Transport Layers Leading to High-Performance Polymer Solar Cells. *J. Mater. Chem. C* **2013**, *1*, 3777–3783.

[215] Devadasan, J. J.; Sanjeeviraja, C.; Jayachandran, M. Electrodeposition of p-$WS_2$ Thin Film and Characterisation. *J. Cryst. Growth* **2001**, *226*, 67–72.

[216] Britnell, L.; Ribeiro, R. M.; Eckmann, A.; Jalil, R.; Belle, B. D.; Mishchenko, A.; Kim, Y.-J.; Gorbachev, R. V; Georgiou, T.; Morozov, S. V; et al. Strong Light-Matter Interactions in Heterostructures of Atomically Thin Films. *Sci.* **2013**, *340* , 1311–1314.

[217] Delphine, S. M.; Jayachandran, M.; Sanjeeviraja, C. Review of Material Properties of (Mo/W)$Se_2$-Layered Compound Semiconductors Useful for Photoelectrochemical Solar Cells. *Crystallogr. Rev.* **2011**, *17*, 281–301.

[218] Pathak, V. M.; Patel, K. D.; Pathak, R. J.; Srivastava, R. Improved Photoconversion from $MoSe_2$ Based PEC Solar Cells. *Sol. Energy Mater. Sol. Cells* **2002**, *73*, 117–123.

[219] Chen, D.; Chen, W.; Ma, L.; Ji, G.; Chang, K.; Lee, J. Y. Graphene-like Layered Metal Dichalcogenide/graphene Composites: Synthesis and Applications in Energy Storage and Conversion. *Mater. Today* **2014**, *17*, 184–193.

[220] Snaith, H. J. Perovskites: The Emergence of a New Era for Low-Cost, High-Efficiency Solar Cells. *J. Phys. Chem. Lett.* **2013**, *4*, 3623–3630.

[221] Yue, G.; Wu, J.; Xiao, Y.; Huang, M.; Lin, J.; Lin, J.-Y. High Performance Platinum-Free Counter Electrode of Molybdenum Sulfide-Carbon Used in Dye-Sensitized Solar Cells. *J. Mater. Chem. A* **2013**, *1*, 1495–1501.

[222] Du, G.; Guo, Z.; Wang, S.; Zeng, R.; Chen, Z.; Liu, H. Superior Stability and High Capacity of Restacked Molybdenum Disulfide as Anode Material for Lithium Ion Batteries. *Chem. Commun.* **2010**, *46*, 1106–1108.

[223] Chang, K.; Chen, W. L-Cysteine-Assisted Synthesis of Layered $MoS_2$/Graphene Composites with Excellent Electrochemical Performances for Lithium Ion Batteries. *ACS Nano* **2011**, *5*, 4720–4728.

[224] Chen, S.; Qiao, S.-Z. Hierarchically Porous Nitrogen-Doped Graphene–$NiCo_2O_4$ Hybrid Paper as an Advanced Electrocatalytic Water-Splitting Material. *ACS Nano* **2013**, *7*, 10190–10196.

[225] Pham, V. H.; Kim, K.-H.; Jung, D.-W.; Singh, K.; Oh, E.-S.; Chung, J. S. Liquid Phase Co-Exfoliated $MoS_2$–graphene Composites as Anode Materials for Lithium Ion Batteries. *J. Power Sources* **2013**, *244*, 280–286.

[226] Wulfmeier, H.; Albrecht, D.; Ivanov, S.; Fischer, J.; Ulrich, S.; Bund, A.; Fritze, H. High-Temperature Thin-Film Calorimetry: A Newly Developed Method Applied to Lithium Ion Battery Materials. *J. Mater. Sci.* **2013**, *48*, 6585–6596.

[227] Zhao, X.; Mai, Y.; Luo, H.; Tang, D.; Lee, B.; Huang, C.; Zhang, L. Nano-$MoS_2$/poly (3,4-Ethylenedioxythiophene): Poly(styrenesulfonate) Composite Prepared by a Facial Dip-Coating Process for Li-Ion Battery Anode. *Appl. Surf. Sci.* **2014**, *288*, 736–741.

[228] Jing, Y.; Zhou, Z.; Cabrera, C. R.; Chen, Z. Metallic $VS_2$ Monolayer: A Promising 2D Anode Material for Lithium Ion Batteries. *J. Phys. Chem. C* **2013**, *117*, 25409–25413.

[229] Xie, J.; Zhang, J.; Li, S.; Grote, F.; Zhang, X.; Zhang, H.; Wang, R.; Lei, Y.; Pan, B.; Xie, Y. Controllable Disorder Engineering in Oxygen-Incorporated $MoS_2$ Ultrathin Nanosheets for Efficient Hydrogen Evolution. *J. Am. Chem. Soc.* **2013**, *135*, 17881–17888.

[230] Voiry, D.; Yamaguchi, H.; Li, J.; Silva, R.; Alves, D. C. B.; Fujita, T.; Chen, M.; Asefa, T.; Shenoy, V. B.; Eda, G.; et al. Enhanced Catalytic Activity in Strained Chemically Exfoliated $WS_2$ Nanosheets for Hydrogen Evolution. *Nat Mater* **2013**, *12*, 850–855.

[231] Voiry, D.; Salehi, M.; Silva, R.; Fujita, T.; Chen, M.; Asefa, T.; Shenoy, V. B.; Eda, G.; Chhowalla, M. Conducting $MoS_2$ Nanosheets as Catalysts for Hydrogen Evolution Reaction. *Nano Lett.* **2013**, *13*, 6222–6227.

[232] Guo, C. X.; Dong, Y.; Yang, H. Bin; Li, C. M. Graphene Quantum Dots as a Green Sensitizer to Functionalize ZnO Nanowire Arrays on F-Doped $SnO_2$ Glass for Enhanced Photoelectrochemical Water Splitting. *Adv. Energy Mater.* **2013**, *3*, 997–1003.

[233] Politano, A.; Chiarello, G. Periodically Rippled Graphene on Ru(0 0 0 1): A Template for Site-Selective Adsorption of Hydrogen Dimers via Water Splitting and Hydrogen-Spillover at Room Temperature. *Carbon N. Y.* **2013**, *61*, 412–417.

[234] Wang, B.; Sun, Q.; Liu, S.; Li, Y. Synergetic Catalysis of CuO and Graphene Additives on $TiO_2$ for Photocatalytic Water Splitting. *Int. J. Hydrogen Energy* **2013**, *38*, 7232–7240.

[235] Wang, Y.; Guo, X.; Dong, L.; Jin, G.; Wang, Y.; Guo, X.-Y. Enhanced Photocatalytic Performance of Chemically Bonded SiC-Graphene Composites for Visible-Light-Driven Overall Water Splitting. *Int. J. Hydrogen Energy* **2013**, *38*, 12733–12738.

[236] Xie, G.; Zhang, K.; Guo, B.; Liu, Q.; Fang, L.; Gong, J. R. Graphene-Based Materials for Hydrogen Generation from Light-Driven Water Splitting. *Adv. Mater.* **2013**, *25*, 3820–3839.

[237] Chen, G.; Li, D.; Li, F.; Fan, Y.; Zhao, H.; Luo, Y.; Yu, R.; Meng, Q. Ball-Milling Combined Calcination Synthesis of $MoS_2$/CdS Photocatalysts for High Photocatalytic H2 Evolution Activity under Visible Light Irradiation. *Appl. Catal. A Gen.* **2012**, *443–444*, 138–144.

[238] Zhuang, H. L.; Hennig, R. G. Single-Layer Group-III Monochalcogenide Photocatalysts for Water Splitting. *Chem. Mater.* **2013**, *25*, 3232–3238.

[239] Choi, C.; Feng, J.; Li, Y.; Wu, J.; Zak, A.; Tenne, R.; Dai, H. $WS_2$ Nanoflakes from Nanotubes for Electrocatalysis. *Nano Res.* **2013**, *6*, 921–928.

[240] Li, Y.; Wang, H.; Xie, L.; Liang, Y.; Hong, G.; Dai, H. $MoS_2$ Nanoparticles Grown on Graphene: An Advanced Catalyst for the Hydrogen Evolution Reaction. *J. Am. Chem. Soc.* **2011**, *133*, 7296–7299.

[241] Li, Y.; Li, Y.-L.; Araujo, C. M.; Luo, W.; Ahuja, R. Single-Layer $MoS_2$ as an Efficient Photocatalyst. *Catal. Sci. Technol.* **2013**, *3*, 2214–2220.

[242] Lin, T.-W.; Liu, C.-J.; Lin, J.-Y. Facile Synthesis of $MoS_3$/carbon Nanotube Nanocomposite with High Catalytic Activity toward Hydrogen Evolution Reaction. *Appl. Catal. B Environ.* **2013**, *134–135*, 75–82.

[243] Liu, Y.; Yu, Y.-X.; Zhang, W.-D. $MoS_2$/CdS Heterojunction with High Photoelectrochemical Activity for $H_2$ Evolution under Visible Light: The Role of $MoS_2$. *J. Phys. Chem. C* **2013**, *117*, 12949–12957.

[244] Maeda, K.; Xiong, A.; Yoshinaga, T.; Ikeda, T.; Sakamoto, N.; Hisatomi, T.; Takashima, M.; Lu, D.; Kanehara, M.; Setoyama, T.; et al. Photocatalytic Overall Water Splitting Promoted by Two Different Cocatalysts for Hydrogen and Oxygen Evolution under Visible Light. *Angew. Chemie Int. Ed.* **2010**, *49*, 4096–4099.

[245] Wang, T.; Liu, L.; Zhu, Z.; Papakonstantinou, P.; Hu, J.; Liu, H.; Li, M. Enhanced Electrocatalytic Activity for Hydrogen Evolution Reaction from Self-Assembled Monodispersed Molybdenum Sulfide Nanoparticles on an Au Electrode. *Energy Environ. Sci.* **2013**, *6*, 625–633.

[246] Wu, Z.; Fang, B.; Wang, Z.; Wang, C.; Liu, Z.; Liu, F.; Wang, W.; Alfantazi, A.; Wang, D.; Wilkinson, D. P. $MoS_2$ Nanosheets: A Designed Structure with High Active Site Density for the Hydrogen Evolution Reaction. *ACS Catal.* **2013**, *3*, 2101–2107.

[247] Xiang, Q.; Yu, J.; Jaroniec, M. Synergetic Effect of $MoS_2$ and Graphene as Cocatalysts for Enhanced Photocatalytic $H_2$ Production Activity of $TiO_2$ Nanoparticles. *J. Am. Chem. Soc.* **2012**, *134*, 6575–6578.

[248] Yuan, Y.-P.; Cao, S.-W.; Yin, L.-S.; Xu, L.; Xue, C. $NiS_2$ Co-Catalyst Decoration on $CdLa_2S_4$ Nanocrystals for Efficient Photocatalytic Hydrogen Generation under Visible Light Irradiation. *Int. J. Hydrogen Energy* **2013**, *38*, 7218–7223.

[249] Zhuang, H. L.; Hennig, R. G. Computational Search for Single-Layer Transition-Metal Dichalcogenide Photocatalysts. *J. Phys. Chem. C* **2013**, *117*, 20440–20445.

*The authors declare no conflict of interest*

© 2015 By the Authors; Licensee Borderless Science Publishing, Canada. This is an open access article distributed under the terms and conditions of the Creative Commons Attribution license http://creativecommons.org/licenses/by/3.0

## Abbreviation

TMDCs: Transition metal dichalcogenides; $MX_2$: Metal–dichalcogenides; 2D: Two-dimensional; CVD: Chemical Vapor Deposition;PTCDA: Perylene-tetracarboxylic dianhydride ; MWI: Microwave irradiation; LIB: Li-ion battery;HER: Hydrogen evolution reaction; DFT: Density functional theory ; EDLC: Electric double layer capacitor ; AFM: Atomic Force Microscope; SEM: Scanning electron Microscope; HRTEM: High Resolution Transmission Electron Microscope; $MoS_2$: Molybdenum Disulfide; $WS_2$: Tungsten Disulfide; $MoSe_2$: Molybdenum Diselenide ; $MoTe_2$: Molybdenum Ditelluride; $TaSe_2$: Tantalum Diselenide; $NbSe_2$: Niobium Diselenide; $NiTe_2$: Nickel Ditelluride; BN: Boron Nitride; $Bi_2Te_3$: Bismuth Telluride; $WSe_2$: Tungsten Diselenide; GaS: Gallium sulfide; GaSe: Gallium selenide; $WTe_2$: Tungstn Ditelluride; GaTe: Gallium Telluride; InSe: Indium Selenide; $HfS_2$: Hafnium Disulfide; $PtS_2$: Platinum Disulfide; PEC: Photoelectrochemical cell; CTO: Conductive transparent oxide;

## Biography

**1. Dr. Dattatray J. Late**

Dr. Dattatray Late has completed his BSc, MSc and PhD (2008) degree in Physics from University of Pune (India). After completing his PhD with Prof. D. S. Joag, he has joined as a DST Post-doctoral Fellow on Nanoscience & Technology with Prof. C. N. R. Rao at JNCASR, Bangalore (2008-2010). Then after he moved to Department Materials Science and Engineering, Northwestern University (USA) Chicago, as an IUSSTF Postdoctoral Fellow to work with Prof. Vinayak P. Dravid (2010-2012). Currently he holds a position of DST Ramanujan National Fellow and AcSIR Assistant Professor at CSIR-National Chemical Laboratory. His current research interest includes "Synthesis of Atomically thin nanosheets of graphene and 2D inorganic layered materials for Nanoelectronics device applications such as Transistors, Photodetector, gas sensors, supercapacitor, Light Emitting Diode, Field Emission and catalyst for water splitting etc. and Raman spectroscopy". He has authored or co-authored more than 60 research papers in international journals. His current google scholar h-index is 20 with total citations >1700. He is also reviewers for various journals in ACS, Wiley, RSC, sciencedirect and Nature publishing group etc.

**2. Dr. Chandra Sekhar Rout:**

Dr. Chandra Sekhar Rout is a DST Ramanujan Fellow at Indian Institute of Technology Bhubaneswar, India. He received his B.Sc. (2001) and M.Sc. (2003) degree from Utkal University and his Ph.D. from Jawaharlal Nehru Centre for Advanced Scientific Research, India (2008) followed by his postdoctoral research works at National University of Singapore and Purdue University, USA. His research interests include nanoscience and nanotechnology, nanomaterials for electronic devices, energy storage devices, chemical and biosensors etc. He has authored or co-authored more than 50 research papers in

international journals. His current google scholar h-index is 21 with total citations >2100. He is also reviewers for various top journals in ACS, Wiley, RSC, Sciencedirect etc.

**3. Disha Chakravarty**

Ms.Disha Chakravarty graduated (B.Tech) in Electronics and communication engineering (ECE) from Hitkarini College of Engineering and Technology (2010) Jabalpur (India). She obtained her Master's degree (M.Tech) in Nanotechnology from Rajiv Gandhi Technical University (UTD) in 2012, Bhopal (India). There she gained enough experience in synthesis of various nanomaterials and their application in Field-Emission based devices. Currently she joined CSIR-NCL Pune, India as a Project Assistant Staff under the guidance of Dr. D. J. Late on DST sponsored project.

**4. Satyajit Ratha**

Mr. Satyajit Ratha is a project assistant at the School of Basic Sciences, Indian Institute of Technology Bhubaneswar, India. Prior to joining IIT Bhubaneswar, he received his Bachelor of Science, First Class Honours from Utkal University, in 2008 and Master of Science from Ravenshaw University in 2010. Satyajit's research interests include two dimensional semiconductors, nanostructure synthesis, applications, energy storage devices and supercapacitors.